The Graduate Institute of Science and Engineering

M.Sc. Thesis in Electrical and Computer Engineering

MODELING AND SIMULATION OF THIN-FILM SOLAR CELLS

by

Bashir Abdullahi BABA

July 2014
Kayseri, Turkey

MODELING AND SIMULATION OF THIN-FILM SOLAR CELLS

By

Bashir Abdullahi BABA

A thesis submitted to

the Graduate Institute of Science and Engineering

of

Meliksah University

in partial fulfillment of the requirements for the degree of

Master of Science

in

Electrical and Computer Engineering

July 2014
Kayseri, Turkey

APPROVAL PAGE

This is to certify that I have read the thesis entitled “Modeling and Simulation of Thin-film Solar Cells” by Bashir Abdullahi Baba and that in my opinion it is fully adequate, in scope and quality, as a thesis for the degree of Master of Science in Electrical and Computer Engineering, the Graduate Institute of Science and Engineering, Melikşah University.

____

July 8, 2014 Yrd. Doç. Dr. Gökhan ÖZGÜR
Supervisor

I certify that this thesis satisfies all the requirements as a thesis for the degree of Master of Science.

____

July 8, 2014 Prof. Dr. Murat Uzam
Department Chair

Examining Committee Members

Title and Name		Approved
Yrd. Doç. Dr. Gökhan ÖZGÜR	July 8, 2014	____________________
Yrd. Doç. Dr. MahmutKarakaya	July 8, 2014	____________________
Yrd. Doç. Dr. ErcanSevkat	July 8, 2014	____________________

It is approved that this thesis has been written in compliance with the formatting rules laid down by the Graduate Institute of Science and Engineering.

____

Prof. Dr. M. Halidun Keleştemur
Director

July 2014

MODELING AND SIMULATION OF THIN-FILM SOLAR CELLS

Bashir Abdullahi BABA

M.S. Thesis in Electrical and Computer Engineering
July 2014

Supervisor: Yrd. Doç. Dr. Gökhan ÖZGÜR

ABSTRACT

The amorphous silicon and crystalline silicon (a-Si/c-Si) heterojunction solar cell is the technological solution for the photovoltaic (PV) market because it performs well and has low production cost. This technology employs a high efficient c-Si cell technology and low cost thin-film a-Si:H technology in single structure.

However, the influence of band offsets at the a-Si and c-Si interface is one of the crucial issues in the operation and design of these cells. The band offsets give rise to potential barriers that could impose limitations for the photocarrier collection which in turn affects the PV properties of the solar cell.

In this thesis, a solution to the above-mentioned issue has been proposed by designing a structure with graded band gap layers of a-Si_xGe_{1-x}:H inserted in between a-Si:H(n) and c-Si(p) to replace the a-Si:H(i) layer in a simple heterojunction with intrinsic thin layer (HIT). The graded layers help in reducing the band offsets values in a graded way which can make photocarrier transportation from one side to the other easier by making a staircase from lower energy level to higher, which in turn increases the current drawn from the cell and also the total efficiency.

Furthermore, the proposed structure has been optimized using the AFORS-HET simulation software by varying the thicknesses and doping concentrations of the various layers to yield an efficiency of 32.07%.

Keywords: Photovoltaics, a-Si thin films, solar cells, band offsets.

İNCE-FİLM GÜNEŞ PİLLERİNİN MODELLENMESİ VE SİMÜLASYONU

BashirAbdullahi BABA

Yüksek Lisans Tezi – Elektrik veBilgisayarMühendisliği

Temmuz 2014

Tez Danışmanı: Yrd. Doç. Dr. Gökhan ÖZGÜR

ÖZ

Amorf silisyum ve Kristal silisyum (a-Si/c-Si) heteroeklem güneş pilleri, yüksek performansları ve düşük maliyetlerinden dolayı fotovoltaik (PV) pazar için teknolojik bir çözümdürler. Bu teknoloji, yüksek verimliliğe sahip kristal silisyum (c-Si) teknolojisi ile düşük maliyetli hidrojen katkılı amorf silisyum (a-Si:H) teknolojisini tek yapıda kullanır.

Bununla birlikte, a-Si ve c-Si arayüzündeki bant farklının etkisi bu güneş pillerinin çalışma ve tasarımında önemli bir sorun olarak karşımıza çıkmaktadır. Bu bant farkının sonucunda oluşan potansiyel bariyer, foto (ışıkla oluşan) elektrik yüklerinin toplanmasında sınırlama getirmektedir ve bunun sonucunda güneş pilinin fotovoltaik özellikleri etkilenmektedir.

Bu tez çalışmasında yukarıda belirtilen probleme çözüm üretmek için, katkısız ince katmanlı basit heteroeklem (HIT) yapılarda bulunan a:Si:H(i) katmanın yerine geçmek üzere enerji bant aralığı basamaklandırılmış olan a-Si_xGe_{1-x}:H katmanların a:Si:H(n) ile c:Si(p) arasında kullanan bir yapı önerilmektedir. Basamakladırılmış katmanlar sayesinde, bant farkları dereceli olarak azaltılacak ve bu yolla foto elektrik yüklerinin düşük enerji seviyesinden merdiven şeklinde yüksek enerjiye çıkmasıyla bir taraftan diğer tarafa taşınması kolaylaşmış olacaktır. Bunun sonucunda, pilden elde edilen akım ve toplam verimlilik yükselecektir.

Buna ilaveten, önerilen yapının çeşitli katmanlarına ait kalınlıkları ve katkı oranlarının Afors-hetsimülasyon yazılımı ile optimizasyonu yapılarak %32.07 verimlilikte bir güneş pili tasarlanmıştır.

AnahtarKelimeler: Fotovoltaik, a-Si ince filmler, güneş pilleri, bant farkı.

DEDICATION

I dedicate my thesis work to my parents and my entire family at large for their tireless support, love, prayers, and words of encouragement since childhood to date.

ACKNOWLEDGEMENT

I would like to acknowledge and extend my sincere gratitude to my beloved and most cherished governor, a philanthropist of the highest order, a credible leader, worthy of emulation, hardworking and dedicative governor His Excellency Dr. Rabiu Musa KWANKWASO, who provides me with a full scholarship to study Master's degree in abroad.

Sincere gratitude to my honorable supervisor, Yrd. Doç. Dr. Gökhan ÖZGÜR, for his kind guidance and constant effort to make me work for perfection. His patience and immense knowledge has been of a constant source of motivation.

I am grateful to everyone who have helped me directly and indirectly with information, motivation and support, particularly my friends, colleagues and brothers "19 masters students of Melikşah University" I am grateful indeed.

Lastly, I want to thank my family for their continuous support, inspiration and sacrifice, I thank my wife for her patient and understanding during the period of my study, thank you so much and God bless you all.

TABLE OF CONTENTS

ABSTRACT iii
ÖZ iv
DEDICATION v
ACKNOWLEDGMENT vi
TABLE OF CONTENTS vii
LIST OF TABLES ix
LIST OF FIGURES x
TABLE OF SYMBOLS xiii
CHAPTER 1 INTRODUCTION 1
1.1 Energy and Solar Energy 1
1.2 Solar Cells 2
1.2.1 PV Market 2
1.2.2 PV Materials 3
1.3 Crystalline Silicon Solar Cells 4
1.4 Thin-Film Silicon Technology 5
1.4.1 Amorphous Silicon Solar Cells 5
1.4.2 Microcrystalline Silicon Solar Cells 6
1.5 a-Si:H/c-Si Heterojunction Solar Cells 7
1.6 Outline of the Thesis 8
CHAPTER 2 PHYSICS OF SOLAR CELLS 9
2.1 Solar Spectrum 9
2.2 Solar Cell Device Structure 11
2.3 P-N Junction Diode 12
2.4 Solar Cell Device Operation 14
2.5 I-V Curve and Solar Cell Characteristics 16

2.5.1 Solar Cell I-V Curve 16
2.5.2 Solar Cell Characteristics 17
2.6 Solar Cell Set of Equations 19
2.6.1 Poisson's Equation 19
2.6.2 Current-Density Equations 20
2.6.3 Continuity Equations 21
2.6.4 Set of the Equations 22
CHAPTER 3 SIMULATION OF SOLAR CELLS 23
3.1 Overview of the Solar Cell Simulation 23
3.2 Introduction to AFORS-HET Software 23
3.3 Equations for AFORS-HET 25
3.3.1 Optical Simulation 25
3.3.2 Electrical Simulation 26
3.3.3 Basic Recombination Models 28
3.4 Simulation of Simple a-Si:H/c-Si Heterojunction Solar Cells 29
3.4.1 Simple HIT Structure Used for the Simulation 29
3.4.2 Simulation Parameters 30
3.4.3 Simulation Results 30
CHAPTER 4 APPROACHES TO HIGH PERFORMANCE HIT SOLAR CELLS 33
4.1 Proposed Structure 34
4.2 Parameters of a-SiGe:H 35
4.3 Simulation of the Proposed Structure 37
4.3.1 Band Diagrams 37
4.3.2 I-V Curve and Solar Cell Output Parameters 38
4.4 Comparison between Simple HIT and Proposed Structures 38

CHAPTER 5 OPTIMIZATION OF THE STRUCTURE AND DISCUSSIONS 40
5.1 Effects of N-Layer 40
5.1.1 Optimization of N-Layer Thickness 40
5.1.2 Optimization of N-Layer Doping Concentration 43
5.2 Effects of Intrinsic Layer 44
5.2.1 Optimization of I-Layer Thickness 45
5.3 Effects of P- Layer 46
5.3.1 Optimization of P-Layer Thickness 47
5.3.2 Optimization of P-Layer Doping Concentration 49
5.4 Effects of Transparent Conducting Oxides (TCOs) 51
CHAPTER 6 CONCLUSION AND FUTURE WORK 53
REFERENCES 54

LIST OF TABLES

TABLE

3.1 Parameter values for simulation of simple HIT structure 30
4.1 Parameters of a-SiGe:H 35
4.2 Electron affinities and band gaps of different materials 35
4.3 Electron affinities for different band gaps of a-SiGe:H 36
4.4 Comparison Between simple HIT and Proposed structures 39
5.1 Variation of n-layer thickness 40
5.2 Variation of n-doping 43
5.3 Variation of i-layer thickness 45
5.4 Variation of p-layer thickness 47
5.5 Variation of p-doping taking the effect of mobilities into consideration 49
5.6 Optimized parameters 51
5.7 Effects of Transparent Conducting Oxides 51

LIST OF FIGURES

Fig. 1.1 Worldwide solar cell productions (1999 to 2010) 2
Fig. 1.2 Average PV module prices AII Technologies (1980 to 2008) 3
Fig. 1.3 Market share for different types of solar cell in year 2010 4
Fig. 2.1 Solar spectrums for AM0, AM1.5G and AM1.5D used under fair use 2013 .9
Fig. 2.2 Illustration of various AM position and the zenith points 10
Fig. 2.3 Efficiency vs. band gap for AM0 and AM1.5G spectrums...........................11
Fig. 2.4 Schematics of a typical p-n junction Solar cell 11
Fig. 2.5 Depletion region created at p-n junction...13
Fig. 2.6 Band diagrams representing solar cell operation at dark and under light.....15
Fig. 2.7 Current I-V characteristics of solar cell under dark and illumination 17
Fig. 2.8 I-V curve, power curve and some parameters of solar cell 18
Fig. 3.1 Graphical Interface of AFORS-HET 24
Fig. 3.2 Simple Structure of a-Si:H/c-Si Heterojunction 29
Fig. 3.3 Band diagram of the simple HIT structure under dark 30
Fig. 3.4 Band diagram of the simple HIT structure under illumination 31
Fig. 3.5 I-V characteristics for the simple HIT structure 31
Fig. 3.6 Conduction band offset zoomed from figure 3.3..32
Fig. 4.1 Band offsets between a-Si:H and c-Si 33
Fig. 4.2 Proposed Structure 34
Fig. 4.3 Graph of electron affinity against band gap...36
Fig. 4.4 Band diagram for the proposed structure...37
Fig. 4.5 I-V curve for the proposed structure..38
Fig. 5.1 Variation of V_{OC} with n-layer thickness 41
Fig. 5.2 Variation of J_{SC} with n-layer thickness 41

Fig. 5.3 Variation of fill factor with n-layer thickness 42
Fig. 5.4 Variation of efficiency with n-layer thickness 42
Fig. 5.5 Variation of Voc with n-layer doping 43
Fig. 5.6 Variation of Jsc with n-layer doping 43
Fig. 5.7 Variation of fill factor with n-layer doping 44
Fig. 5.8 Variation of efficiency with n-layer doping 44
Fig. 5.9 Variation of Voc with i-layer thickness 45
Fig. 5.10 Variation of Jsc with i-layer thickness 45
Fig. 5.11 Variation of fill factor with i-layer thickness 46
Fig. 5.12 Variation of efficiency with i-layer thickness 46
Fig. 5.13 variation of Voc with p-layer thickness 47
Fig. 5.14 Variation of Jsc with p-layer thickness 48
Fig. 5.15 Variation of fill factor with p-layer thickness 48
Fig. 5.16 Variation of efficiency with p-layer thickness 48
Fig. 5.17 Variation of Voc with p-layer doping 49
Fig. 5.18 Variation of Jsc with p-layer doping 50
Fig. 5.19 Variation of fill factor with p-layer doping 50
Fig. 5.20 Variation of efficiency with p-layer doping 50

TABLE OF SYMBOLS

μc-Si:H	Hydrogenated microcrystalline silicon
a-Si:H	Hydrogenated amorphous silicon
c-Si	crystalline silicon
nc-Si	Nanocrystalline silicon
mc-Si	Multicrystalline silicon
HJ	Heterojunction
SHJ	Silicon heterojunction
HIT	Heterojunction with intrinsic thin layer
LPCVD	Low pressure chemical vapor deposition
VHF-GD	Very-high frequency glow-discharge
PECVD	Plasma enhanced chemical vapor deposition
VHF	Very high frequency
ZnO	Zinc oxide
TCO	Transparent conductive oxide
ITO	Indium tin oxide
J_{SC}	Short circuit current density
V_{OC}	Open circuit voltage
FF	Fill factor
η	Efficiency
I-V	Current voltage
EQE	External quantum efficiency
AM	Air mass
C-V	Capacitance voltage
C-T	Capacitance temperature

CHAPTER ONE

INTRODUCTION

1.1 ENERGY AND SOLAR ENERGY

The world demand of energy is growing very fast, it was found that the total energy consumption in the world is expected to increase by 0.7 – 1.4% yearly under the period of 2008 to 2035, depending on the chosen energy scenario [1,2]. This increasing demand of energy is due to (i) a fast growing world population (there will be 9 billion people in 2050 against 6 billion in 2000 [3]) and (ii) rapid economic growth in some of the countries like China and India [1,4]. Nowadays, fossil fuels dominated the world source of energy, (i.e. oil (40%), coal (33%) and natural gas (27%) [5]).in 2008, fossil fuels have a market share of 81% of the total world energy consumption [1]. But due to its limited resources and environmental impact, this consumption cannot be sustained in the long term [1,2,6], and new sources of energy generation have to be explored. Among the new sources, renewable energy in general and solar energy in particular are highly promising candidates [6, 7].

Solar energy conversion can be sub divided into two different technologies: solar thermal and Solar Cell or photovoltaic (PV). In solar thermal, energy from sunlight is converted into heat for domestic use or for conversion to electricity in large size concentrated solar power plants, while in solar cell; energy from sunlight is directly converted into DC electricity. For the rest of this thesis, only solar cell will be taken into consideration.

1.2 SOLAR CELL

Solar cell is a solid state device that converts photons of light directly into DC electricity, using the photovoltaic effect .The photovoltaic effect refers to the generation of a potential difference at the junction of two different materials in response to visible or other radiation. Photovoltaic effect was first discovered by Becquerel in 1839 [8]. The first working solar cell was constructed in 1883 by Charles Fritts [9] with efficiency of 1%. After lasting striving for near a whole century, solar cell efficiency finally saw 20% under AM 1.5G and 37% under concentration [10-12].

1.2.1 PV Market

Over the past years, the market share of PV in global energy has increased substantially. In 2010, an estimated record solar cell production of 23.9 GW was realized; a 123% increase over 2009 [13,14]! In 2009, a cell production of 10.5 – 12.2 GW was realized, which was a 50% increase over 2008 [13,15], leading at that time to a total globally installed power exceeding 20 GW [16]. Figure 1.1 shows the world solar cell productions growth from 1999-2010.

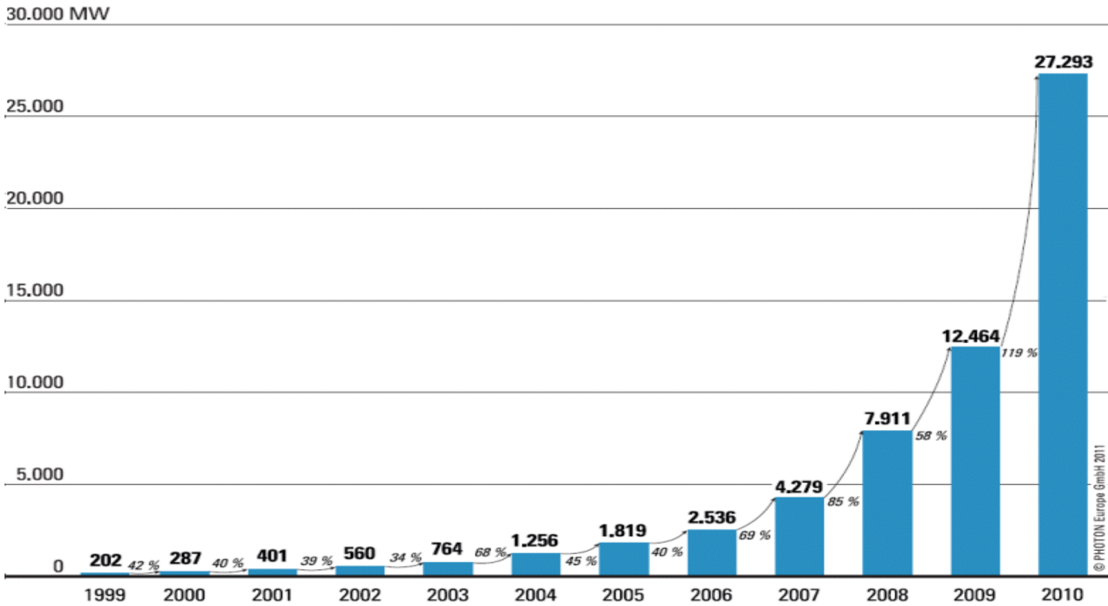

Figure 1.1 Worldwide solar cell productions (1999-2010) [13]

Recently, EPIA (together with A.T. Kearney) has developed three different growth scenarios for PV until 2020 [17,18]; one baseline scenario and two alternative scenarios, leading to a higher market share for PV. The two alternative scenarios are the ‘accelerated scenario’ and the ‘paradigm shift scenario’, leading to a 6% and 12% contribution, respectively, to the electricity consumption in Europe by the year 2020[18].
The 2010 world energy consumption is approximately equal to 500 EJ (1 EJ = 10^{18} J)[1]. The solar constant, which is defined as the average amount of energy from the sunlight incident on a plane perpendicular to the direction of the photons, outside the earth’s atmosphere, is equal to 1366 W/m2 [19]. This leads to a total irradiation on the earth’s surface in the order of 1024 J, which is roughly 2000 times the actual world energy consumption. This clearly demonstrates that solar energy has, at least in theory, the potential to supply the global energy demand. Figure 1.2 shows the average price of PV module.

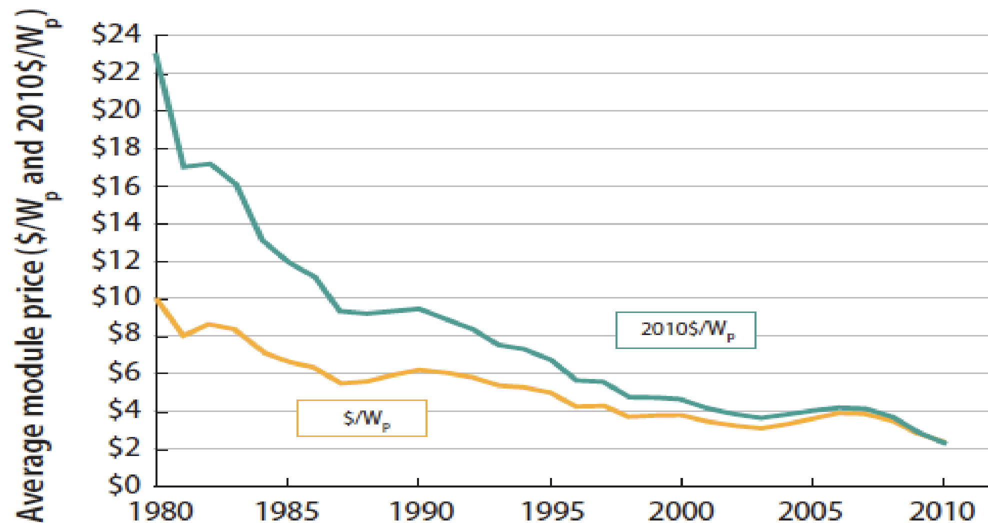

Figure 1.2 average PV module prices, AII Technologies (1980-2008) [5]

1.2.2 PV Materials

Semiconductor materials that are most commonly used for solar cell are, amongst others: Si, Ge, GaAs, CdTe, CdSe, Copper Indium (Gallium) Selenide (CI(G)S),III-V compound semiconductor materials and several organic materials. But some of these materials include toxic (like Cd) while some are rare (like In and Te). This makes them unsuitable for long

term large scale production. The most suitable material is silicon, which is non-toxic and second most abundant element on earth. Figure 1.3 shows the market share for different solar cells in 2010.The market share of crystalline silicon(c-Si) based solar cells was 87% [14].Crystalline silicon solar cell has this impressive market share because it combines state-of-the-art production techniques with high module efficiencies, off-the-shelf manufacturing equipment and processing with low capital costs.

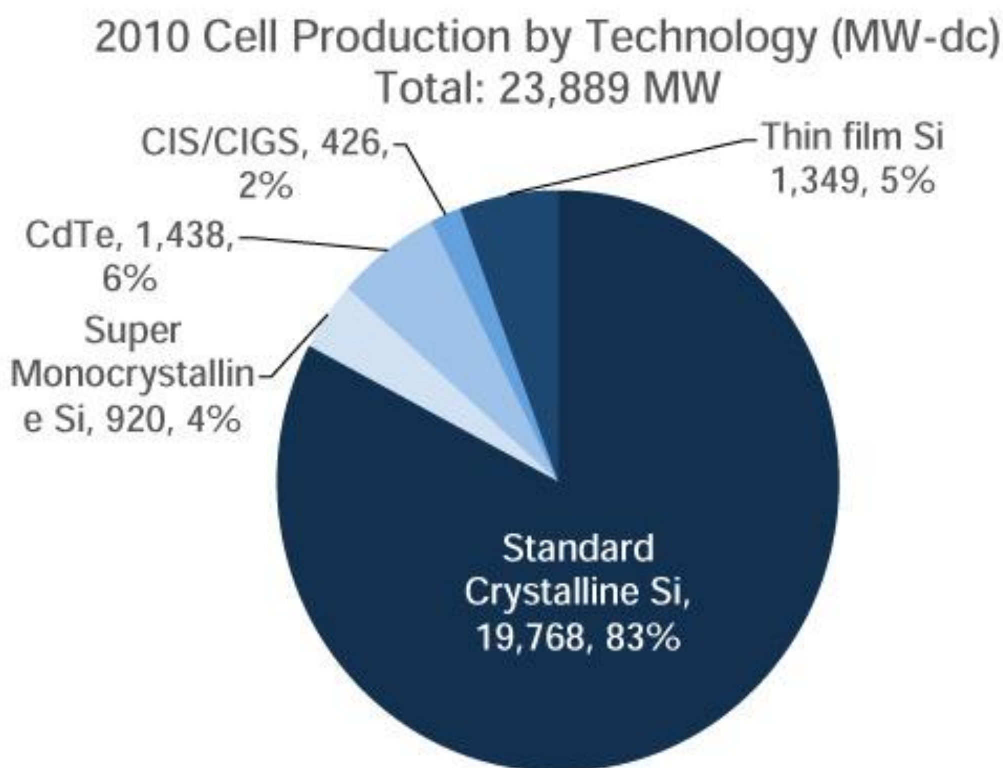

Figure 1.3Market share for different types of solar cells in year 2010 [14]

1.3 CRYSTALLINE SILICON SOLAR CELLS

Crystalline silicon solar cell was first fabricated in 1954 by Bell laboratories [20] with a conversion efficiency of 6%. Since then, the efficiencies have been increasing. Currently the world record efficiency for c-Si solar cells is 25.0% [21]. C-Si solar cells show higher efficiency compared to any other materials, and they have little degradation. On the other hand, conventional c-Si solar cells suffer from high (~800-900°C) processing temperatures and material usage. Both aspects are obviously detrimental for the production costs. For

crystalline silicon solar cells, the production cost of wafers (including both mono-crystalline and multi-crystalline) is the major obstacle for the technology. Today, 25% to 45% of the cost of the crystalline silicon based module comes from the cost of Si wafer itself.

Generally, cost reduction in cell processing is achieved by the use of (i) cheaper substrates, like multicrystalline Si (mc-Si), metallurgical silicon and ribbon Si, and (ii) thinner wafers. The main disadvantages of mc-Si are the lower efficiencies (the record cell efficiency on mc-Si equals 20.3% [22]) and degradation of material quality during high T processing. While the disadvantage of using a thinner wafers (100µm) is related to warping issues and even breaking associated with high temperature processing, in addition to material losses related to sawing. Due to the reasons described above, low temperature processing may (partly) solve the main issues related to the use of cheaper c-Si based materials.

1.4 THIN-FILM SILICON TECHNOLOGY

An alternative cheap technology to c-Si solar cells are thin film silicon based solar cells (consisting of hydrogenated amorphous silicon (a-Si:H) and/or hydrogenated microcrystalline silicon (µc-Si:H)).

1.4.1 Amorphous Silicon (a-Si:H) Solar Cell

The first a-Si:H based thin film solar cell was fabricated in 1976 at RCA Laboratories, with an efficiency of 2.4% [23]. Ever since that time the efficiencies have been improving and currently, the stabilized efficiency for a single junction a-Si:H based solar cell equals to 10.1% [24]. This cell has an intrinsic a-Si:H absorber layer with a thickness of 180 nm and was made by plasma enhanced chemical vapor deposition(PECVD) at a plasma excitation frequency of 40.68 MHz instead of the standard radio frequency (rf) of 13.56 MHz and at a deposition rate of 0.18 nm/s. The cell was deposited on doped ZnO:B which was made by Low Pressure Chemical Vapor Deposition (LPCVD).

a-Si:H has different material properties compared to c-Si. Firstly, its band gap is around 1.8 eV, which is higher than that of c-Si (1.1 eV). The lack of long-range order leads to a relaxation of momentum conservation in electronic transitions [25] and thereby to a higher absorption coefficient. This permits the use of much less material which is a strong

potential in cost reduction. Another aspect of reducing the cost is the low fabrication temperatures of a-Si:H based solar cells typically around 200°C (much lower than that of c-Si). This enables the use of cheap and flexible substrates, such as plastics [26] and Al foil [27].

However the main disadvantages of a-Si:H based solar cells are (i) the lower efficiencies compared to c-Si (which is due to the higher defect density of the material) and (ii) light induced degradation due to the Staebler-Wronski effect [28], leading to a relative decrease in efficiency up to approximately 20% for single junction a-Si:H solar cells[29].

Another advantage of a-Si:H is the possibility to fabricate multijunction solar cells, using multiple absorber layers with a different band gap. The most commonly fabricated multijunction thin film Si solar cells consist of an a-Si:H as top cell and a μc-Si:H as bottom cell [30,31]. Triple junction solar cells, in which the absorber layers consist of a-Si:H (top cell), a-SiGe:H or μc-Si (middle cell) and a-SiGe:H or μc-Si:H (bottom cell), are also studied [32-35].

1.4.2 Microcrystalline Silicon Solar Cells

μc-silicon (also called nanocrystalline silicon (nc-Si)) can be considered as a two-phase material, which consists of small crystallites (about 20nm in diameter) embedded in an a-Si:H matrix [36]. Its band gap is around 1.1 eV, similar to that of c-Si. The material was first described in 1968 by Veprek and Marecek [37]. The first solar cell with an intrinsic absorber layer consisting of μc-Si:H was fabricated at the Institute of Micro engineering (IMT) in Neuchâtel, Switzerland by Meierin 1994 [38] with a conversion efficiency of 4.6%. Currently, the highest reported efficiency for a single junction solar cell with a μc-Si:H absorber layer equals 10.1% [39]. For a-Si:H/ μc-Si:H double junction (tandem) solar cells, the stabilized record efficiency is equal to 11.9% [40]. For a-Si:H/μc-Si:H/μc-Si:H triple junction solar cells, a stabilized record efficiency of 12.5% has been obtained [34]. All record efficiencies listed in this section are independently confirmed and can be found in [41]

1.5 a-Si:H/c-Si HETEROJUNCTION SOLAR CELLS

A very successful approach in which a-Si:H and c-Si are combined are a-Si:H/c-Si heterojunction (SHJ) solar cells. In this technology, the base material, in which the sunlight is absorbed, consists of c-Si and the emitter is made by depositing thin films consisting of a-Si:H. The use of thin films which serve as emitter has several advantages. First of all, these thin films can easily be fabricated at temperatures below 200°C, while in conventional c-Si solar cells the junction formation is usually be done using a thermal diffusion step, in which very high temperatures (800-900°C)are needed [42]. These lower fabricating temperatures (i) enable the use of thinner wafers (<100μm), avoiding warping issues associated with high temperature processing and (ii) strongly reduce the thermal budget of the production process.

a-Si:H/c-Si heterojunction devices was first made by Fuhs *et al.* in 1974 [43] while SHJ solar cell was made first in 1983 by Okuda *et al.* [44] with a conversion efficiency of 9%. The concept of depositing a thin intrinsic layer on the c-Si wafer before depositing the oppositely doped emitter was first introduced by Sanyo in 1991[45], this leads to lower recombination losses at the amorphous-crystalline interfaces which will give a better cell performance. This breakthrough encouraged many research groups to start investigating the concept of SHJ solar cells. Ever since the early 1990s, Sanyo has been leading the efficiency tables for SHJ cells. In 2009, they achieved a conversion efficiency of 23% with an open circuit voltage (V_{OC}) of 729 mV on a cell area of 100.5 cm^2 [46].

SHJ solar cells have a lower temperature coefficient than conventional c-Si solar cells, that is to say its nominal power output at typical operating temperatures (60-80°C) compared to standard test conditions (STC; 1000 W/m^2, 25°C and AM1.5 illumination [47]) is more favorable [48]. Another important advantage compared to conventional c-Si cells is the possibility to deposit a thin intrinsic layer before depositing the doped a-Si:H emitter and BSF layers. This concept was first introduced by Sanyo [45] and their excellent results have made many other groups to focus on this approach as well. Due to a reduced density of defect states at the a-Si:H/c-Si interface, this concept allows the V_{OC} values to exceed 720mV [46,49].

1.6 OUTLINE OF THE THESIS

This thesis consists of six chapters. Chapter 2 which is next to this chapter, introduces the fundamental back ground on solar cells such as device structure, p-n junction, operation of solar cell and characterization of solar cell. chapter 3 discusses the simulation of solar cell, introduces the AFORS-HET simulation software and simulation of simple HIT structure using AFORS-HET was performed. Chapter 4 is the main chapter of the thesis, it gives our approach in getting a high efficient solar cell, where a novel structure was designed and simulated. Chapter 5 focuses on the optimization of the designed structure, the thicknesses and doping concentrations of various layers was varied and optimized. Finally, Chapter 6 gives conclusion and future work.

CHAPTER TWO

PHYSICS OF SOLAR CELL

2.1 SOLAR SPECTRUM

Helium is created from hydrogen by nuclear fusion, this process powers the sun. It causes the temperature of the sun's core to be 1.57×10^7 K and that of sun's surface to be ~5578 K. The radiations from the sun coming at such high temperatures can be approximated as blackbody radiations. The solar spectrum and the corresponding solar intensity reaching the earth's surface are different than the spectrum reaching the outer space. The air mass coefficients (AM) have been defined for comparing the solar module performance under standard test conditions. Air mass helps define the length of the path through the atmosphere the radiation would have to travel in relation to the shortest length if the sun was in the apex. For solar radiations incident at a zenith angle (z) relative to the normal to the earth's surface, the air mass coefficient can be defined as:

$$\mathrm{AM} = \frac{1}{\cos z} \tag{2.1}$$

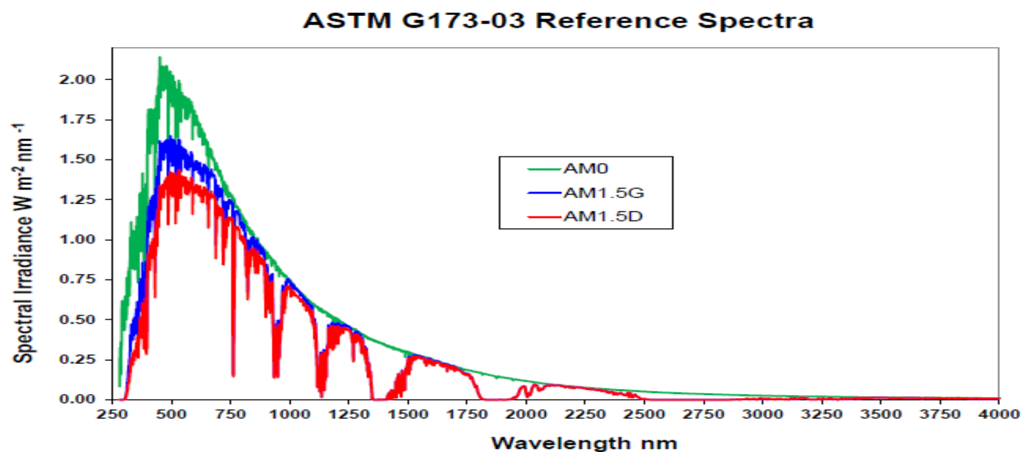

Figure 2.1 Solar Spectrums for AM0, AM1.5G and AM1.5D Used under fair use, 2013

The standard air masses for space, terrestrial and concentrated sunlight are defined as AM0, AM1.5G (global) and AM1.5D (direct), respectively and the corresponding spectrums are shown in Fig. 2.1 [50]. The corresponding incident intensities for AM0, AM1.5G and AM1.5D are ~1356 W/m^2, ~1003 W/m^2 and ~887 W/m^2 respectively. The zenith angles for the different air mass solar spectrums are represented in Fig. 2.2 [51].

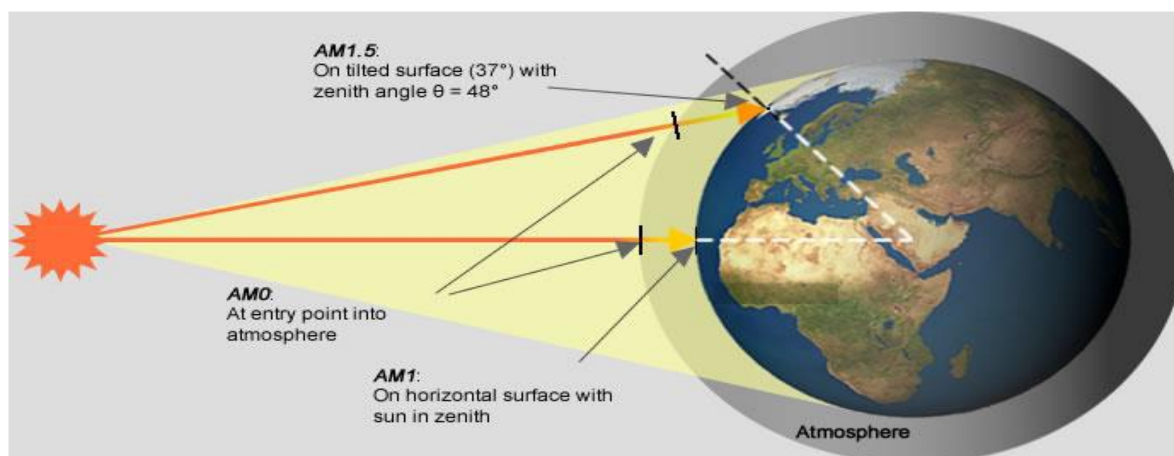

Figure 2.2 Illustration of various air mass (AM) positions and the zenith point Used under fair use, 2013.

The theoretically calculated efficiencies for AM1.5G and AM0 spectrums as a function of semiconductor band gap are shown in the Fig. 2.3 [52]. The optimal band gap for AM1.5G is 1.4eV and that of AM0 is1.6eV. These theoretical efficiencies did not include the losses due to surface recombination, absorption coefficients, limited cell thickness and the influence of material properties which relate to various recombination losses in a solar cell.

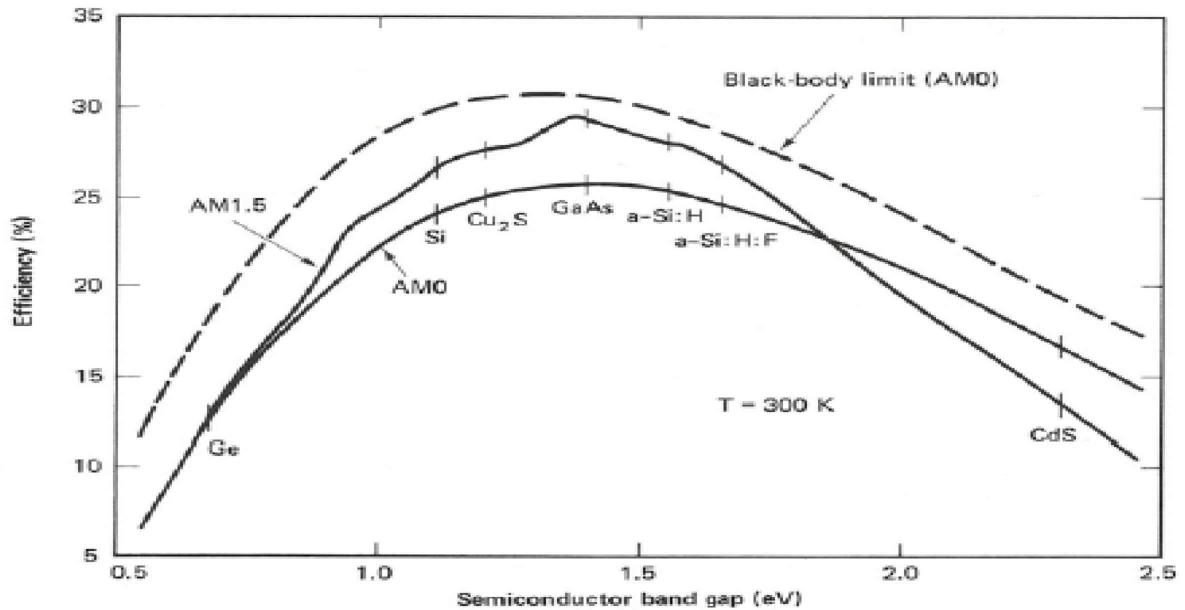

Figure 2.3 Efficiency vs. band gap for AM0 and AM1.5G spectrums. Used under fair use, 2013

2.2 SOLAR CELL DEVICE STRUCTURE

Solar cells are usually formed by creating p-n junctions region in a semiconductor. A typical p-n junction based solar cell is shown in Fig. 2.4. It has five basic components: emitter, base, the backside metal contact, the front side metal grids, and the antireflection layer.

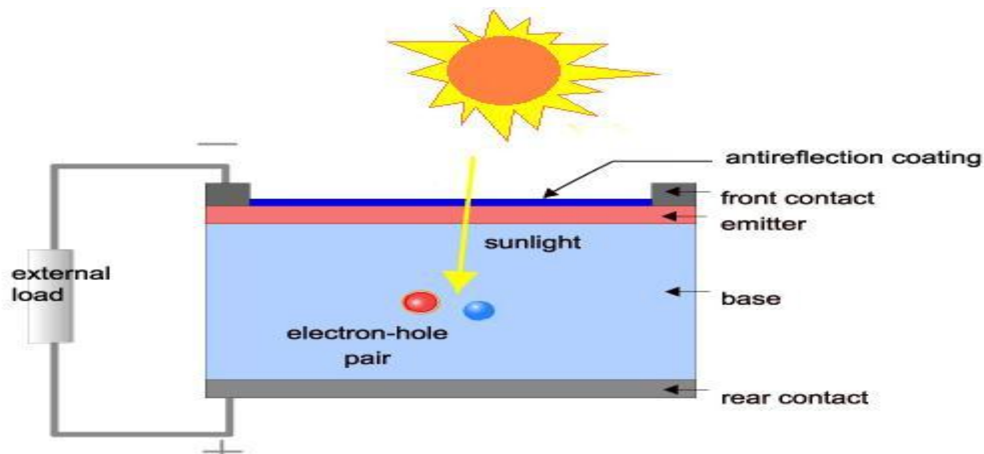

Figure 2.4 Schematics of a typical p-n junction solar cell

Always, the base and emitter are made by two different (p- or n-) types of materials, so as to form a p-n junction. The layer that is illuminated first is called the emitter layer and is usually more heavily doped and thinner than the base layer. Most of the light absorption in a solar cell happens in the thicker and lightly doped base layer. Lower doping ensures higher diffusion coefficients and higher minority carrier lifetime, which also improves the carrier diffusion length. Moreover, lower doping in the base increases the depletion region in the base, which can aid in carrier collection due to the presence of electric field. However, when doping is too low it will increase the dark current, which may significantly degrade the device performance.

2.3 P-N JUNCTION DIODE

P-n junction is not only the basis for solar cells, but also the fundamental device structure of many other electronics devices, like LEDs, transistors, and integrated circuits. When a p-type and an n-type material are brought together in intimate contact, a p-n junction is said to be created, as shown in Fig. 2.5. Since there is higher concentration of holes in p-region and higher concentration of electrons in n-region, holes diffuse from p-side to n-side. Similarly, electrons diffuse to p-side to n-side. As the carriers (electrons and holes) move to the other side of the junction, they leave exposed charges behind on dopant atom sites, which are fixed in the crystal lattice. Negative ion cores are exposed on the p-side while positive ion cores are exposed on n-side. An electric field (ϵ)is then formed between the positive and negative ion cores and also a "built in" potential (V_{bi})due to the electric field(ϵ)is formed at the junction as well. This region is called the “depletion region", since the field quickly sweeps free carriers out, and the region is depleted of free carriers.

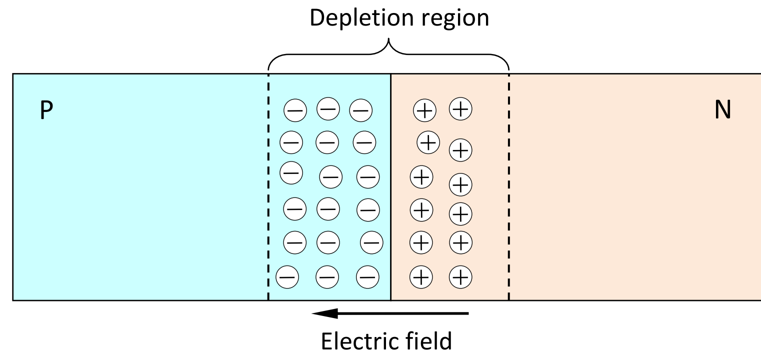

Figure 2.5 Depletion region created at p-n junction.

Despite the establishment of electric field, which creates an obstacle to the diffusion of carriers, some of the majority carriers can still diffused to the other side. Once a majority carrier crosses the junction, it becomes a minority carrier. It will continue to diffuse away from the junction and travel a distance on average equal to the diffusion length before it recombines. The current created by this diffusion of carriers across the junction is called **diffusion current**. While for minority carriers which reach the edge of the depletion region, they are swept across it by the electric field ϵ. This current is called the **drift current**, and is usually limited by the number of minority carriers generated thermally. In equilibrium state, the drift current and the diffusion current cancel each other out and the overall current from the device is zero.

When applying a positive voltage to the p-type or a negative voltage to the n-type materials (forward bias), an electric field with opposite direction to that in the depletion region will be created across the device, which will reduce the net electric field in the depletion region. This disturbs the equilibrium at the junction, and reduces the barrier to the diffusion of carriers, which will result in increase in diffusion current. The drift current which is limited by the number of minority carriers however remains the same. Hence if the p-n junction is connected to an external circuit, a net current will flow under forward bias.

In reverse bias, the electric field at the junction increases due to the voltage applied across the device. The higher electric field in the depletion region decreases the probability that carriers can diffuse from one side of the junction to the other, hence the diffusion current decreases slightly. Similar as that in forward bias, the drift current is relatively the same.

2.4 SOLAR CELL DEVICE OPERATION

In a single-junction solar cell, incident light photons that have energies greater than the band-gap energy of the cell's material gets absorbed while the light photons with energies lower than the band-gap energy is transmitted and pass through the cell without absorbing. When a photon is absorbed, it makes an electron from the valence band to jump to the conduction band, thereby creating an electron-hole pair (EHP). These generated EHP diffuse through the quasi-neutral region until they reach the p-n junction where the drift mechanism begins to dominate the carrier transport due to the built-in electric field and sweeps away the carriers across the depletion region to become majority carriers. Electrons generated in the p-side travel towards the n-side and holes generated in the n-side travel towards the p-side. This redistribution of carriers sets up a potential difference, Voc which is created due to the splitting of the thermal equilibrium Fermi-level (E_F) into minority electron quasi-Fermi level (E_{Fn}), and minority hole quasi-Fermi level (E_{Fp}). This difference gives rise to the open-circuit voltage, $V_{OC} \approx \frac{\left(E_{Fn} - E_{Fp}\right)}{q}$. This separation in the quasi-Fermi level can be seen in the band-diagram shown in the Fig. 2.6.

The electrons generated move towards the cathode at the top and the holes moves towards the anode at the bottom. Under illumination, the electron-hole pair generation might not significantly increase the majority carrier concentration; however, the minority carrier concentration is significantly increased and hence, due to the concentration gradient developed in the quasi-neutral region the diffusion current dominates. The flow of generated minority carriers essentially defines the direction of the light induced current density or the photo generated current density (J_{ph}) flowing from n-terminal to p-terminal. Collection of all the negative charges on the n-side and the positive charges on the p-side creates a light-induced forward bias to the solar cell. As a result of this forward bias in the presence of an external load, diode current begins to flow in the opposite direction to the photo generated current and is typically referred as the diode dark current, J_{dark}. It is important to minimize the dark current as it reduces the photo generated current. Diode current measurements reveal important information about the recombination mechanism prevalent in the solar cell, which may limit its performance.

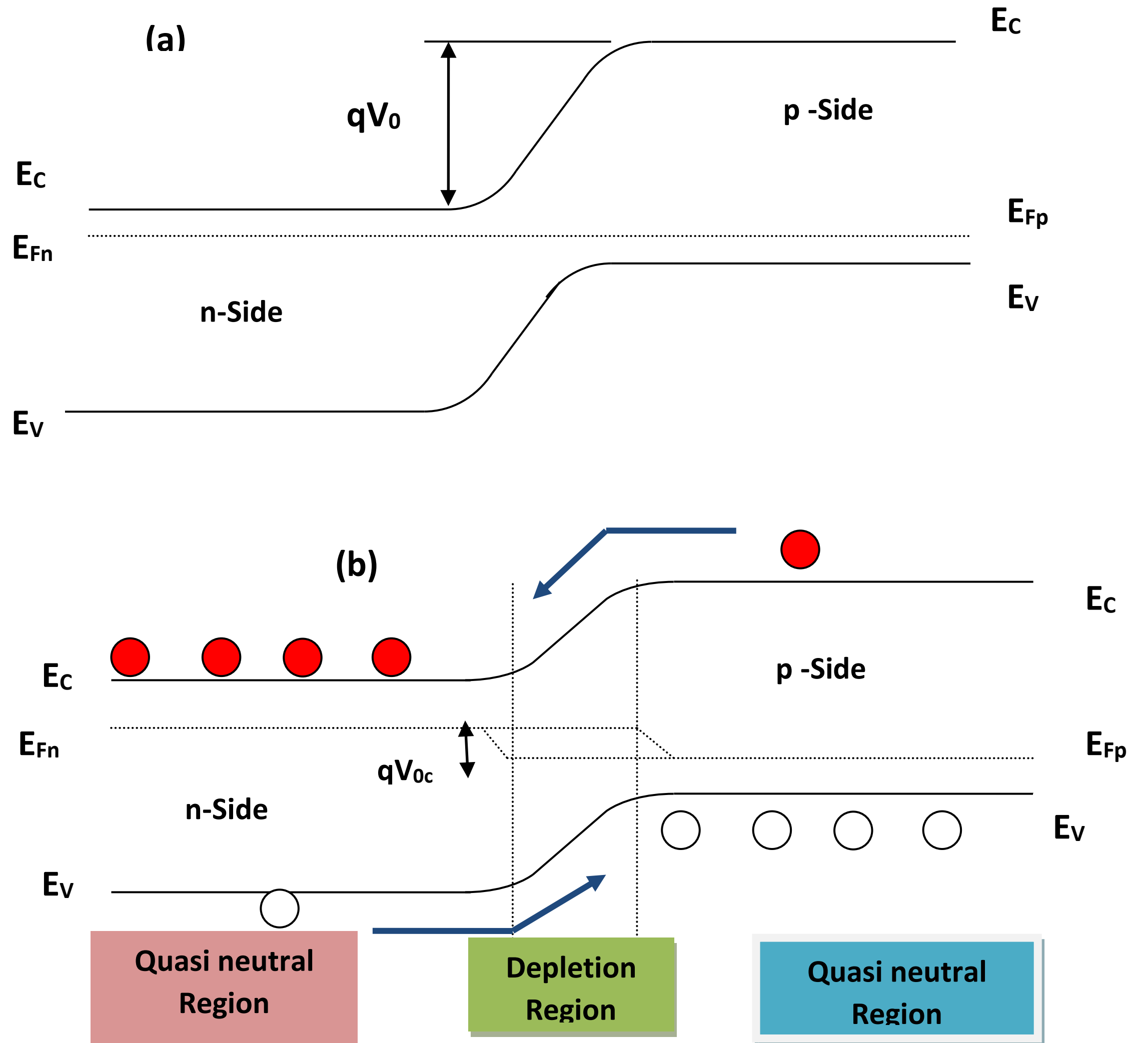

Figure 2.6 Band-diagrams representing solar cell operation (a) at equilibrium, and (b) Under light.

One of the most important solar cell material parameters is the minority carrier diffusion length (L_e *or* L_h), which depends on the minority carrier lifetime (τ_e *or* τ_h) and minority carrier diffusion coefficient (D_e *or* D_h). Their relationship is given by:

$$L = \sqrt{D\tau} \tag{2.2}$$

$$\frac{D}{\mu} = \frac{kT}{q} \tag{2.3}$$

These parameters are very important when designing the cell thicknesses and doping. The idea is to maximize the diffusion length in order to allow the minority carriers to reach their respective majority carrier sides for collection to the external circuit. The cell thicknesses are designed in accordance with the diffusion lengths of the minority carrier. These parameters depend on the doping concentration.

2.5 SOLAR CELL I-VCURVE AND CHARACTERISTICS

2.5.1 Solar Cell I-V Curve

Unlike normal p-n junctions, solar cell operates under light illumination. Therefore the *I-V* curve of solar cell is the superposition of *I-V* curve of a normal p-n junction diode in the dark plus a light-generated current. Qualitatively, the light has the effect of shifting the p-n junction's dark *I-V* curve down into the fourth quadrant where power can be extracted from the diode.

The relationship of current *I* through an ideal diode (p-n junction) as a function of voltage *V* can be expressed by the "ideal diode law" as follow:

$$I = I_O \left(e^{\frac{qv}{kT}} - 1 \right) \tag{2.4}$$

Where I_O is the "dark saturation current", q is electron charge, k is Boltzmann's constant, and T is the absolute temperature (K). The dark saturation current I_O is very important parameter for diode and it reflects the recombination in a device.

For solar cells the ideal diode law becomes:

$$I = I_O \left(e^{\frac{qv}{kT}} - 1 \right) - I_L \tag{2.5}$$

Where, I_L is the light-generated current. The effect of light on the *I-V* characteristics of a p-n junction, can be shown in Fig. 2.7

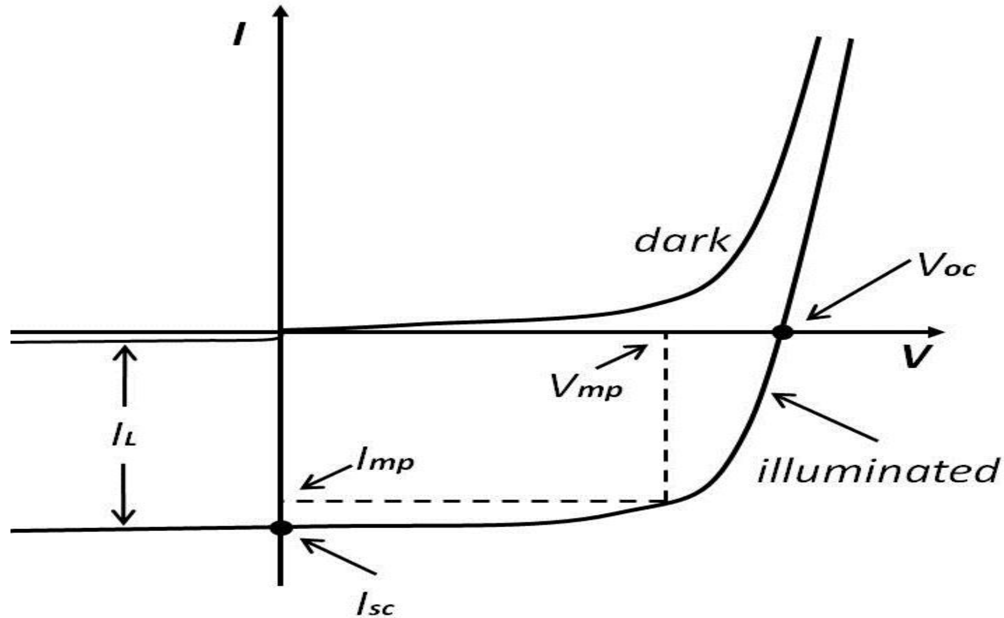

Figure 2.7 Current-voltage (IV) characteristic of a solar under illumination and under no illumination or dark.

2.5.2 Solar Cell Characteristics

There are four important parameters of solar cells that can be derived from *I-V* curve. They are: the short-circuit current (I_{SC}), the open-circuit voltage (V_{OC}), the fill factor (*FF*), and the efficiency (η). As shown on the I-*V* curve in Fig. 2.8.

I. The **short-circuit current (I_{SC})** is the current flowing through the solar cell when the voltage across the cell is zero, i.e. when the solar cell is short circuited. It is due to the generation and collection of light-generated carriers. So ideally, by setting V in equation (2.5) to be zero, the I_{SC} is equal to the light-generated current ($I_{SC} = I_L$), and is the largest current that can be drawn from the solar cell.

II. The **open-circuit voltage (V_{OC})** *is* the maximum voltage available from a solar cell, which occurs when current is zero (when the cell is open circuited). That is, by setting the net current *I* in equation (2.5) to be equal to zero, we have the ideal value of V_{OC} as:

$$V_{OC} = \frac{KT}{q} ln\left(\frac{I_L}{I_O} + 1\right) \tag{2.6}$$

The above equation shows that V_{OC} depends on the light generated current I_L and saturation current I_o of the solar cell. But since I_L has a small variation, then the saturation current I_o has the key effect on V_{OC}, which may vary by orders of magnitude for different solar cells.

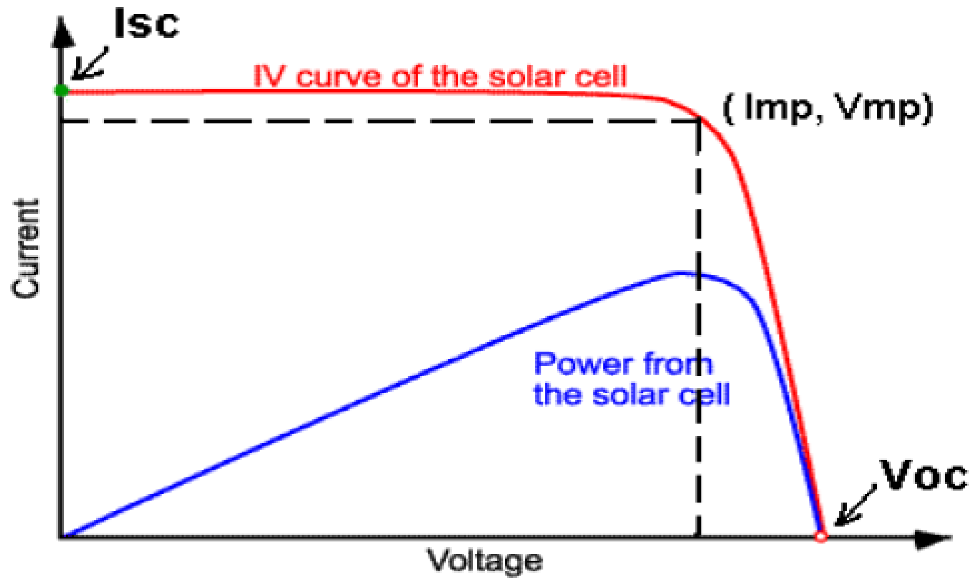

Figure 2.8 Current-voltage (*I-V*) curve, power curve and some parameters of a solar cell.

Although I_{SC} and V_{OC} are the maximum current and voltage for a solar cell, but there is no power at that point (i.e. the output power of the cell at these two extreme points is zero). Hence they are not suitable for operation. The power output of a solar cell for any operating point can be expressed as the rectangle area in the *I-V* curve, indicated in Figure 2.8. There exists one particular operating point (V_{mp}, I_{mp}), which maximizes the power output.

III. **Fill factor (*FF*)** is a parameter that relates the maximum power of a solar cell. It is a measure of the "squareness" of the *I-V* curve, and is defined as the ratio of the maximum power of the solar cell to the product of V_{OC} and I_{SC}, is given as follows:

$$FF=\frac{V_{\max}\times I_{max}}{V_{OC}\times I_{SC}} \tag{2.7}$$

IV. **Efficiency (η)** is defined as the ratio of output energy of the solar cell to the input energy of the sunlight:

$$\eta = \frac{P_{\max}}{P_{in}} = \frac{V_{OC} I_{SC} FF}{P_{in}} \tag{2.8}$$

It is the most important and most used parameter to evaluate the performance of a solar cell. The cell efficiency depends on the spectrum and intensity of the incident sunlight and the operation temperature.

2.6 SOLAR CELL SET OF EQUATIONS

The operation of solar cells can be described by a set of equations, just like any other semiconductor device. Solving these equations help to understand the characteristics of ideal solar cells. In this thesis, the equations will be written in one-dimensional form. The three-dimensional form of this equation is similar except that the spatial derivatives are replaced by the divergence of vector quantities (electric field, current density etc.) and the gradient of scalar quantities (concentrations, potentials etc.).

2.6.1 Poisson's Equation

The first to consider is Poisson's equation [53], this equation relates the space charge density ρ to the divergence of the electric field ϵ. In one dimension, it takes the following form:

$$\frac{d\epsilon}{dx} = \frac{\rho}{\varepsilon} \tag{2.9}$$

Where, ε is the material's permittivity. There are several sources that contribute to charge density (ρ) in a semiconductor. Therefore we can express it as:

$$\rho = q\left(p - n + N_D^+ - N_A^-\right) \tag{2.10}$$

Where *p* and *n* are the densities of holes and electrons, and N_A^- and N_D^+ are the densities of ionized acceptors and donors. Since most shallow donors/acceptors, like B or P in Si, are ionized at room temperature [12], then:

$$N_D^+ \approx N_D$$

$$N_A^- \approx N_A \tag{2.11}$$

Where, N_D and N_A are the total density of donors and acceptors.

By combining equations (2.9) and (2.10) above, the Poisson's equation becomes:

$$\frac{d\epsilon}{dx} = \frac{q}{\varepsilon}\left(p - n + N_D - N_A\right) \tag{2.12}$$

2.6.2 Current-Density Equations

Carriers (electrons and holes) could contribute to current by drift and/or diffusion processes.

Drift Current Density: Under the influence of an electric field ϵ, the drift current density due to conduction band electrons will be:

$$J_e = qnv_d = qn\mu_e\epsilon \tag{2.13}$$

Where v_d is the drift velocity and μ_e is the electron carrier mobility which can be defined by the following:

$$\mu = \frac{v_d}{\epsilon} \tag{2.14}$$

A similar equation was given for holes in the valence band as:

$$J_h = qp\mu_h\epsilon \tag{2.15}$$

Diffusion Current Density: For diffusion, the flux of particles is proportional to the negative of the concentration gradient. Therefore we can get the relationship between current density, which is proportional to the flux of charged particles, and the concentration gradient of electrons. In one-dimensional form the relationship is given by the following equation:

$$J_e = qD_e\frac{dn}{dx} \tag{2.16}$$

Where, D_e is a constant known as the diffusion constant. In the same manner, for hole:

$$J_h = qD_h\frac{dp}{dx} \tag{2.17}$$

The drift and diffusion processes are fundamentally related; hence *Einstein relations* give the mobilities and diffusion constants relationship as:

$$D_e = \frac{kT}{q}\mu_e \text{ and } D_h = \frac{kT}{q}\mu_h \tag{2.18}$$

The total current density can be obtained by adding both the drift current density and diffusion current density. The expression for the total current densities of electrons and holes, J_e and J_h becomes:

$$J_e = qn\mu_e \grave{o} + qD_e \frac{dn}{dx}$$

(2.19)

$$J_h = qp\mu_h \grave{o} + qD_h \frac{dp}{dx}$$

2.6.3 Continuity Equations

For a cross-sectional area A and an elemental volume of length δx, the total rate of increase of electrons in this volume is the rate at which the electrons enter minus the rate at which they exit, plus the rate at which they are generated minus recombined in this volume. But the rates of entering and exiting are proportional to the current densities, that is:

$$\text{(Rate of entering)} - \text{(rate of exiting)} = \frac{A}{q}\left\{-J_e(x) - \left[-J_e(x+\delta x)\right]\right\}$$
$$= \frac{A}{q}\frac{dJ_e}{dx}\delta x \tag{2.20}$$

$$\text{(Rate of generation)} - \text{(rate of recombination)} = A\delta x\left(G-U\right) \tag{2.21}$$

Where G is the total generation rate by external processes like illumination, and U is the total recombination rate.

Under steady-state conditions, the total rate of increase of the electrons must be zero, therefore by equating (2.17) and (2.18) we can get:

$$\frac{1}{q}\frac{dJ_e}{dx} = U - G \tag{2.22}$$

Similarly, for holes: $$\frac{1}{q}\frac{dJ_h}{dx} = -(U-G)$$

Subsidiary relations are required for generation rate G and recombination rate U, and expressions for these terms depend on the specific processes involved.

2.6.4 Set of the Equations

From the above equations (2.11), (2.16), (2.19) we have the following basic equations set for solar cell:

$$
\begin{aligned}
&\frac{d\mathcal{E}}{dx} = \frac{q}{\varepsilon}\left(p - n + N_D - N_A\right) \\
&J_e = qn\mu_e \mathcal{E} + qD_e \frac{dn}{dx} \\
&J_h = qp\mu_h \mathcal{E} + qD_h \frac{dp}{dx} \\
&\frac{1}{q}\frac{dJ_e}{dx} = U - G \\
&\frac{1}{q}\frac{dJ_h}{dx} = -(U - G)
\end{aligned}
\qquad (2.23)
$$

These equations form a coupled set of nonlinear differential equations, for which it is not possible to find general analytical solutions, but they can be solved numerically to provide characteristic information about an ideal solar cell.

CHAPTER THREE

SIMULATION OF SOLAR CELLS

3.1 OVERVIEW OF THE SOLAR CELL SIMULATION

Simple analytical models are not sufficient in understanding solar cells because it provides limited information. Computer aided modeling has become a necessary element in designing and analyzing solar cell performance. It allows studying the effects of each parameter on the performance of the device, and investigating the electronic behavior of a semiconductor device. Although there are many numerical software packages for different kinds of solar cells, with different structures or materials, but their fundamental of physics and set of equations are the same. In this thesis AFORS-HET software will be introduced.

3.2 INTRODUCTION TO AFORS-HET SOFTWARE

AFORS-HET (**a**utomat **for s**imulation of **het**erostructures) is a device simulator program for modeling multi-layer homo- or heterojunction solar cells and typical characterization methods in one dimension. It is developed by Helmholtz-Zentrum, Berlin (a research body, specialized on heterojunction researches)

AFORS-HET allows simulating the output of different measurement techniques (e.g. current-voltage (I-V), quantum efficiency (EQE, IQE), capacitance-voltage (C-V), capacitance-temperature (C-T) etc.) for an arbitrary sequence of semiconductor layers and interfaces, with an arbitrary number of defects distributed within different band gaps. It is especially suitable for simulating hetero-junction solar cells.

AFORS-HET solves Poisson and the transport equations for electrons and holes (Equations 2.23 above) in one dimension. It can define a customized numerical module considering impurity and carrier-carrier scattering for crystalline silicon layer. It can also be used to simulate amorphous materials because of its option to specify the defect density of states

(DOS) for all the layers in the structure. The front contact can be treated either as a metal-semiconductor contact (Schottky contact) or as a metal- insulator-semiconductor contact (MIS contact). In AFORS-HET, also three recombination processes are considered, including band-to-band recombination, Auger recombination, and Shockley-Read-Hall recombination.

The set of couple 1D partial differential equations (Eq.2.23) is transformed into nonlinear algebraic equations by the finite differences method. The free electrons and holes densities and the cell potential at each grid-point are independent variables. The resulting nonlinear equations are solved using the Newton-Raphson iteration scheme, thereby requiring a good starting solution. AFORS-HET use the analytical approximations as a starting solution for equilibrium conditions problems, otherwise the last calculated solution serves as a starting solution for the new boundary conditions to be solved.

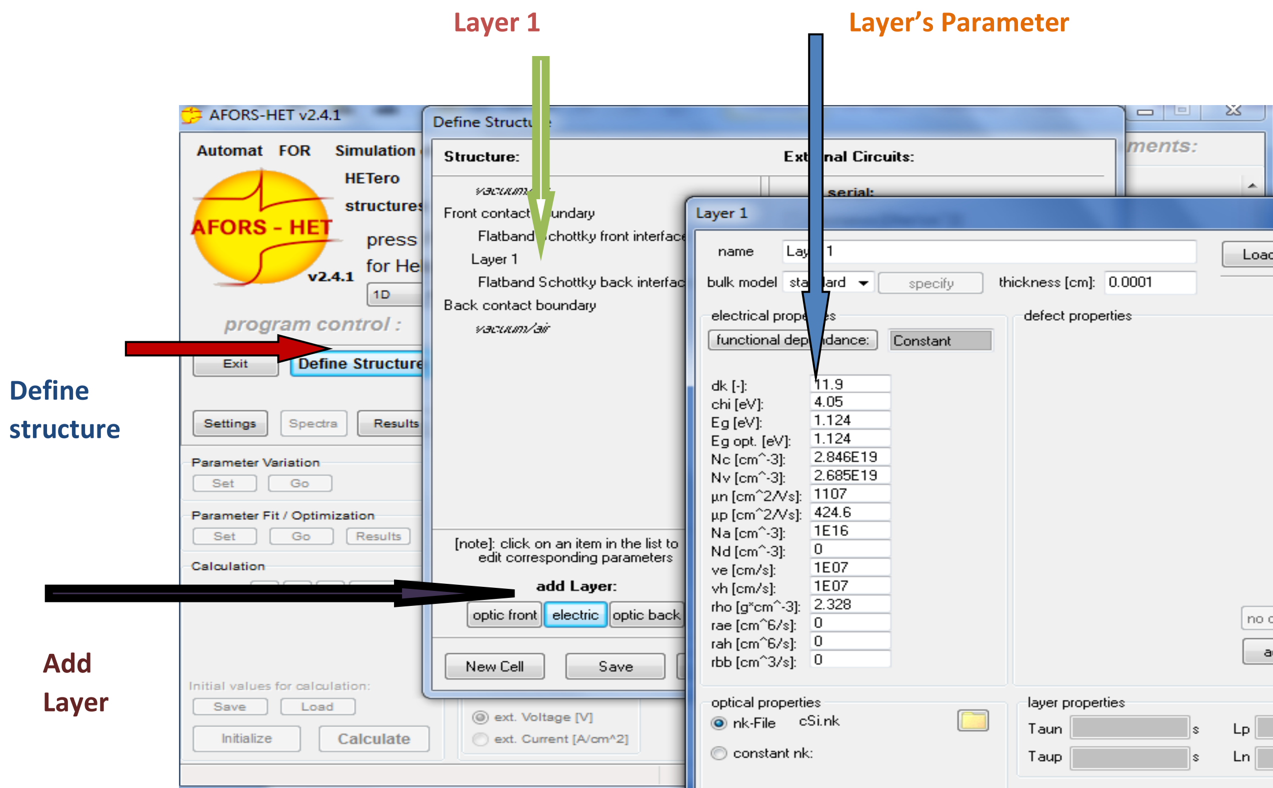

Figure 3.1 Example showing the graphical interface of AFORS-HET.

AFORS-HET also has a friendly graphical user interface (GUI), as shown in Figure 3.1, and it allows an easy visualization of all simulated quantities. The heterostructure and its components (layers, interfaces) can be saved and reloaded. All data can be imported and exported, and thus graphically compared.

3.3 EQUATIONS OF AFORS-HET

The basic equations for optical and electrical calculations in AFORS-HET will be discussed here but the detailed modeling equations can be found in reference [54].

3.3.1 Optical Simulation

There are two different generations for electrons and holes generation rate due to photon absorption,(i) Super bandgap generation for energy of the photon ≥ bandgap and (ii) sub bandgap generation for energy of the photon ≤ bandgap. The sub bandgap generation is calculated in the electrical modeling part, as it depends on local particle densities. The optical super bandgap generation is the same for electrons and holes.

There are two optical models available in AFORS-HET, Lambert-Beer optical absorption model and coherent/incoherent internal multiple reflections optical model. The Lambert-Beer model is more suited to treat c-Si wafer based solar cells. The second model takes coherence effects into account, but is done only for plain surfaces.

Lambert-Beer model this permits multiple forward and backward traveling of light to be taken into account, but it does not consider coherence interference. We can use both changing and constant values of reflectance and absorbance during calculations. The angle travels by the incident light through the layer stack depends on the wavelength of the incident light and can be calculated using Snelliu's law, by the following equation [55]:

$$\gamma(\lambda) = \delta - \arcsin\left[\sin(\delta) \times \frac{1}{n(\lambda)}\right] \tag{3.1}$$

Where γ is the angle of the incident in which the light pass through the layer, δ = 54.7° for textured silicon wafer with <111> pyramids whereas δ = 0° for normal incidence, λ is the wavelength of the incident light and $n(\lambda)$ is the refraction index for the first layer semiconductor at the illuminated side as a function of the wavelength.

It is assumed that all photons of specified wavelength cross the layer stack under distinct angle γ. Photon absorption is then calculated from the spectral absorption coefficient of the semiconductor layer corresponding to the position of the stack, which can be expressed as:

$$\alpha_x(\lambda) = \frac{4\pi k(\lambda)}{\lambda} \tag{3.2}$$

Where, $k(\lambda)$ = extinction coefficient.

The super bandgap electron-hole generation rate for a standard solar spectrum (AM 1.5) incident on the semiconductor layer for single run through is given by:

$$G(x,t) = \int_{\lambda \min}^{\lambda \max} d\lambda \phi(\lambda,t) R(\lambda) A(\lambda) \alpha_x(\lambda) e^{\frac{-\alpha_x(\lambda)x}{\cos(\gamma)}} \tag{3.3}$$

where $\lambda_{\min}$ and $\lambda_{\max}$ are minimum and maximum wavelength of the incident light respectively, is the incoming spectral photon flux and $R(\lambda)$ and $A(\lambda)$ are reflectance and absorbance respectively.

If there is no effect of coherence, the optical generation rate can be calculated as:

$$G(x,t) = G_n(x,t) = G_p(x,t) \tag{3.4}$$

3.3.2 Electrical Simulation

To perform the calculations for electrical simulation all the arbitrary semiconductor layers' equations Poisson's equation and continuity equation for electrons and holes need to be solved. Different physical models are used to describe current in each semiconductor/semiconductor interface and front and backside boundaries. This leads to a system of non linear three dimensional differential equations with respect to time and space derivatives. The system of differential equations is solved for the independent variables, i.e. electron density, hole density and electric potential.

The Poisson's equation can be expressed as:

$$\nabla^2\phi = -\frac{\rho}{\varepsilon} \tag{3.5}$$

Where, ε is the electric permittivity of the material, ϕ is the electric potential across the interface and ρ is the local charge density, which is the sum of all fixed and mobile charges.

Boundary conditions are applied to solve Poisson's equation for electric potential. The boundary condition commonly applied for semiconductor interface is:

$$E\left(0^-\right) = E\left(0^+\right)$$

which implies that, the electric field just before the edge of the interface barrier and electric field just after the edge of the interface barrier are equal, since electric field is a continuous quantity.

In case of DC simulation, the time derivatives are absent, resulting in a simplified system of differential equations. The set of differential equation is then solved for time independent, but position dependent functions. In DC mode, the equations are given as:

$$\begin{aligned} n(x,t) &= n(x) \\ p(x,t) &= p(x) \\ \phi(x,t) &= \phi(x) \end{aligned} \tag{3.6}$$

The one dimensional time independent continuity equation for transport of electrons is given by:

$$-\frac{1}{q}\frac{\partial j_n(x)}{\partial x} = G_n(x,t) - R_n(x,t) \tag{3.7}$$

while,

$$j_n(x) = q\mu_n n(x)\frac{\partial E_{Fn}(x)}{\partial x} \tag{3.8}$$

and

$$E_{Fn} = E_C(x) + KTln\left(\frac{n(x)}{N_C(x)}\right) \tag{3.9}$$

For holes;

$$\frac{1}{q}\frac{\partial j_p(x)}{\partial x} = G_p(x,t) - R_p(x,t) \tag{3.10}$$

with

$$j_p(x) = q\mu_p p(x)\frac{\partial E_{Fp}(x)}{\partial x} \tag{3.11}$$

and

$$E_{Fp} = E_V(x) + KTln\left(\frac{p(x)}{N_V(x)}\right) \tag{3.12}$$

Where $j_p(x)$ and $j_n(x)$ are hole and electron current densities respectively, E_{Fn} and E_{Fp} are the electrons and holes quasi-Fermi levels respectively, μ_n and μ_p are electron and hole mobility respectively, $R_n(x)$ and $R_p(x)$ are electrons and holes recombination rates respectively, E_V and E_C are energies of valence and conduction bands respectively and N_V and N_C are the effective density of states in valence and conduction bands respectively.

3.3.3 Basic Recombination Models

Four basic recombination models are included in AFORS-HET: conduction band to valence band recombination via radiative band to band recombination (R^{BB}), augur recombination (R^{A}), recombination via defect states located within the bandgaps, known as Shockley-Read-Hall recombination (R^{SRH}) and recombination due to the dangling bonds (R^{DB}). Therefore the total recombination in DC simulation is given by;

$$R_{n,p}(x) = R^{BB}(x) + R^{A}(x) + R^{SRH}(x) + R^{DB}(x) \tag{3.13}$$

3.4 SIMULATION OF SIMPLE a-Si:H/c-Si HETEROJUNCTION SOLAR CELL

Simulations of a-Si:H(n)/a-Si:H(i)/c-Si(p) solar cell calculated by AFORS-HET will be presented. The structure based on a p-type wafer will be used because it is more available and cheaper than n-type wafer since microelectronic industries widely use p-type c-Si wafer for device fabrication. However, inferior performance was observed for devices fabricated on c-Si(p) as compared with those on c-Si(n). This was once attributed to the poor back surface field (BSF) effect at the c-Si(p)/a-Si:H(p+) interface due to the large valence band offset there [56,57]. Recently, NREL obtained a decent heterojunction with intrinsic thin layer(HIT) performance on c-Si(p) utilizing the a-Si:H(p+) BSF [58], which suggests that a further investigation is necessary to fully understand the factors that affect the performance of the c-Si(p)-based HIT solar cell,

3.4.1 Simple HIT Structure Used For the Simulation

Figure 3.2 shows the structure and dimension of the layers of the simulated solar cell. The structure is TCO/a-Si:H(n)/a-Si:H(i)/c-Si(p)/Al, the emitter is a-Si:H(n), the absorber is c-Si(p),and the buffer is a-Si:H(i).

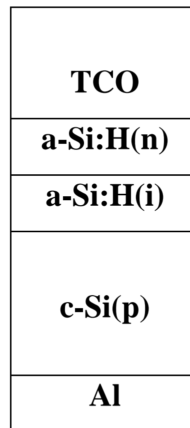

Figure 3.2 structure of the a-Si:H/c-Si solar cell

3.4.2 Simulation Parameters

Table 3.1 shows the parameter values adopted for the solar cell simulation [59], the solar AM1.5 radiation with the density power of 100mW/cm^2 was used as the illuminating source.

Table 3.1 parameter values used for the simulation

Parameters	a-Si:H(n)	a-Si:H(i)	c-Si (p)
Thickness (nm)	10	5	300,000
Dielectric constant	11.9	11.9	11.9
Electron affinity (eV)	3.9	3.9	4.05
Band gap (eV)	1.74	1.72	1.12
Effective conduction/valence band density (cm^{-3})	1E20/1E20	1E20/1E20	2.8E19/1.04E19
Electron/Hole mobility (cm^{2}V^{-1}s^{-1})	20/5	20/5	1040/412
Doping concentration of acceptors/donors (cm^{-3})	0/1E20	0/0	1E16/0
Thermal velocity of electrons/Holes (cms^{-1})	1E7/1E7	1E7/1E7	1E7/1E7

3.4.3 Simulation Results:

The band diagram result for the simulation of the simple HIT structure above is;

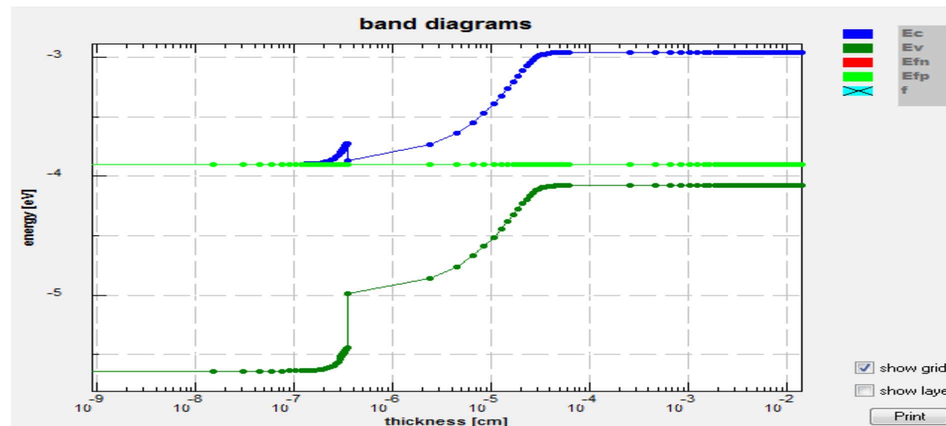

Figure 3.3 Band diagram for the simple HIT structure under dark

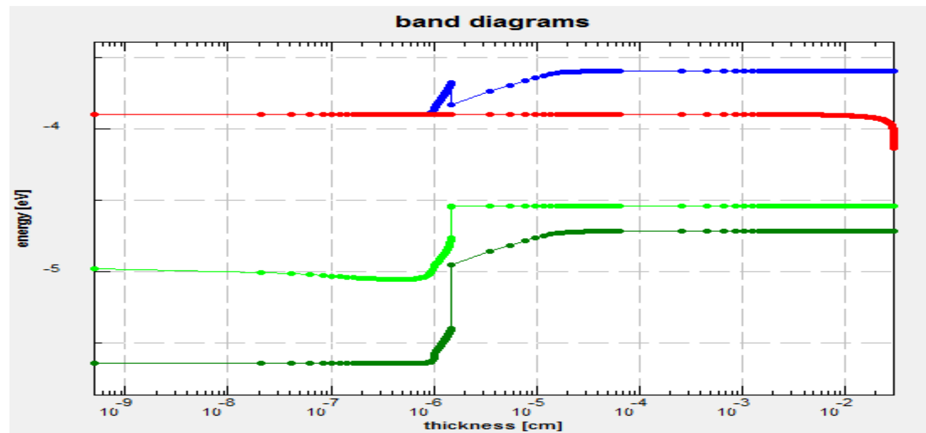

Figure 3.4 Band diagram for the simple HIT structure under illumination

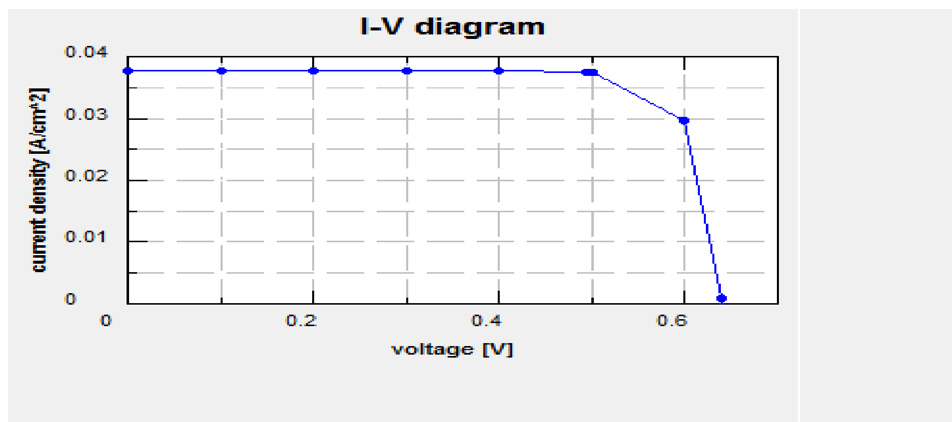

Figure 3.5 IV characteristics for the simple HIT structure

The solar cell output parameters are found to be: V_{OC}=639.8mV, J_{SC}= 37.61mA/cm^2, FF= 76.87%, η= 18.5%. As we can see from the above simulation result, the efficiency is 18.5% only. We study the band diagram of Fig.3.3 carefully and found out that there is a potential barrier between the a-Si:H and c-Si layers (band offsets) which was due to the band gap and electron affinity differences between the two materials. Fig. 3.6 indicates the zoomed out the band offset between c-Si and a-Si:H(i) from the band diagram of Fig. 3.3.

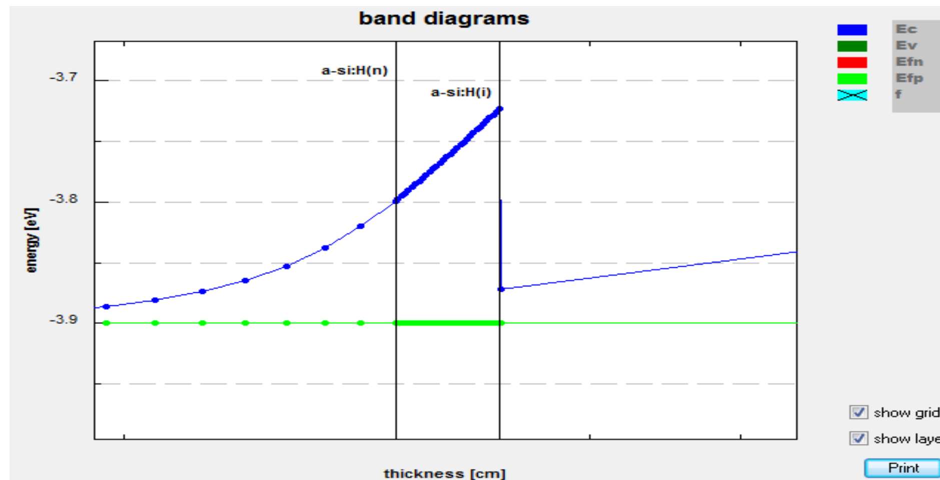

Figure 3.6 Conduction band offset zoomed out from Fig. 3.3

This barrier prevents the electrons that have lower energy than the highest conduction band energy to move from p-type side to n-type side and this reduce the current flow which in turn reduce the efficiency of the solar cell. The electrons can cross the barrier in two ways:

1. Quantum tunneling which occurs when electrons tunnel through the barrier. The corresponding current drawn due to this is called tunneling current.
2. Thermionic emission which occurs when the electrons gain energy and jump over the barrier to the other side.

In this thesis we will concentrate on thermionic emission. But the conduction band offset ΔE_C (which prevents the electrons from moving to the other side) was measured from the above band diagram and found to be 150meV which was too high for the electrons to gain, because normally at room temperature the electron has a thermal energy of 25meV only. Therefore we need to device a means of either reducing the band offset or increasing the electrons energy for us to get more electrons to pass the barrier.

CHAPTER FOUR

APPROACHES TO HIGH PERFORMANCE HIT SOLAR CELLS

One of the most important issues in the operation and design of heterojunction solar cells is the influence of band offsets at the amorphous and crystalline silicon interface which is as a result of the band gaps and electron affinities difference between the two materials as shown and explain in the Band diagram of the simulation of simple HIT structure in the previous chapter. These off sets give rise to potential barriers that could impose limitations for the photo carrier collection, which cause decrease in the short circuit current of the cell and in turn decrease in the efficiency.

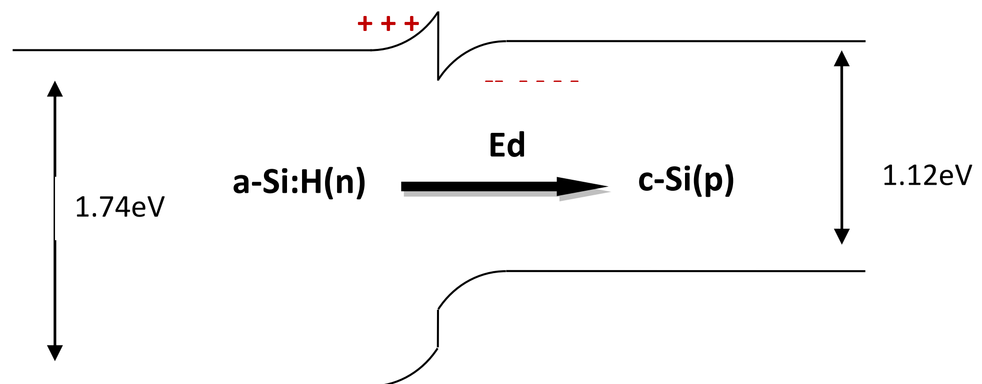

Figure 4.1 Band offset between a-Si:H and c-Si

To obtain higher efficiency HIT solar cell we focus on:

- Grading the band off sets between the amorphous and crystalline silicon interface: This can be achieved by designing a new structure with graded band gap and electron affinity layers inserted in between a-Si:H and c-Si layers which will reduce the $\Delta E_C$to lower values but in a graded form. That is to say we will make a staircase for the electrons.
- Use numerical simulation to optimize the cell parameters of the designed structure.

4.1 PROPOSED STRUCTURE

The band offsets of heterojunction solar cell is due to the bandgap difference between a-Si:H and c-Si materials, it can therefore be reduced by inserting another material with a bandgap value in between that of a-Si:H (1.72 eV) and c-Si (1.12 eV). We proposed a novel structure which consist of graded band gap (1.2 to 1.6eV) of a-SiGe:H alloy as the intrinsic layer in between the a-Si:H(n) and c-Si(p) layers. This is possible because the optical band gap of the a-SiGe:H film can be tailored from 1.78 eV to 1 eV by varying the germanium molar fraction [60].The graded layers will make the photo carrier transportation easier by making something like a stair case for the electrons moving from the p-side to the n-side. As the transportation of electrons increase the current drawn from the cell will also increase. Figure 4.2 shows the structure TCO/a-Si:H(n)/ a-SiGe:H(i)(with graded bandgaps)/c-Si(p)/Al.

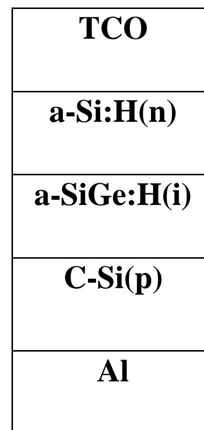

Figure 4.2 Proposed structure

The graded band gap a-SiGe:H intrinsic layer consists of five different layers of a-SiGe:H with a band gaps of 1.2 eV,1.3 eV,1.4 eV,1.5 eV and 1.6 eV each with a thickness of 0.1 nm making the total thickness of the intrinsic layer to be 0.5nm.the layer with a band gap of 1.2 eV will be first deposited on the c-Si(p) layer followed by the one with band gap of 1.3 eV then the layer with 1.4 eV and 1.5 eV lastly the layer with a band gap of 1.6 eV will be next to a-Si:H layer.

4.2 PARAMETERS OF a-SiGe:H

The parameters of a-SiGe:H used in this thesis was given in table 4.1 [60], a-si:H parameters will be used for the remaining parameters necessary for the simulation with AFORS-HET.

Table 4.1 parameters of a-SiGe:H

Parameters	**Values**
Band gap	1.4eV
Electron affinity	4.01eV
Effective conduction/valence band density	1E20/1E20 (cm^{-3})
Electron/hole mobility	60/10 ($cm^2V^{-1}s^{-1}$)

The electron affinities of a-SiGe:H materials for different band gaps were calculated using the parameters in [60]. The values were found by plotting a graph of electron affinity against band gap of a-Si:H, a-SiGe:H and that of c-Si of Table 4.2, this is because all the band gaps and electron affinities of the a-SiGe:H are in between that of the a-Si:H and c-Si. So from the straight line graph we can get the electron affinity for a given band gap.

Table 4.2 electron affinity and band gaps of the materials

Material	Band gap	Electron affinity
a-Si:H	1.74	3.9
a-SiGe:H	1.4	4.01
c-Si	1.12	4.05

Corresponding electron affinity for a given band gap can be found from a plot of band gap against electron affinity using the data in table 4.2. The plot is shown in Fig. 4.3.

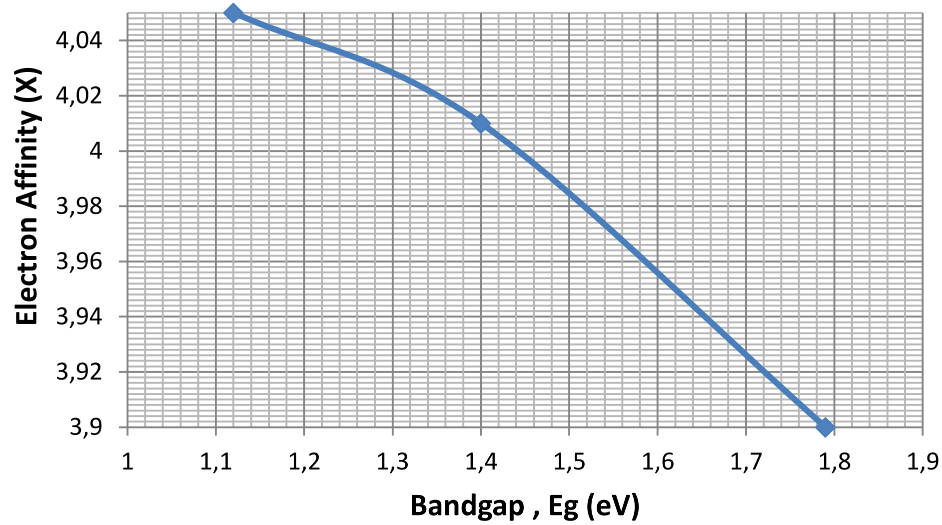

Figure 4.3 graph of electron affinities against band gaps

Table 4.3 Electron affinity for different band gaps of a-SiGe:H

Band gap (eV)	Electron affinity (eV)
1.2	4.04
1.3	4.03
1.4	4.01
1.5	3.98
1.6	3.93

4.3 SIMULATION OF THE PROPOSED STRUCTURE

The proposed structure was simulated with the above parameters using AFORS-HET software, the result of the simulation was shown below:

4.3.1 Band Diagrams

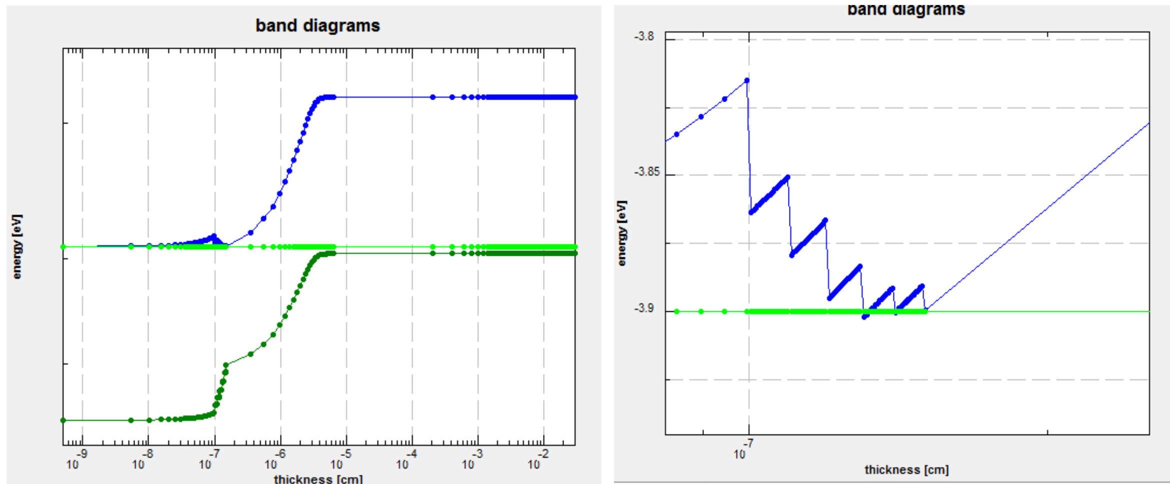

Figure 4.4 Band diagrams for the graded structure

As seen from the zoomed band diagram, the band offset was graded. Initially the value of the band offset was measured to be 150meV but now it was graded to 30meV each, this will make the electrons easier to move, though electrons at room temperature has 25meV of energy they need a little more energy to jump over the band offset. Fortunately the solar cell is working under sun not at room temperature this will give the electrons extra 5meV to overcome the barrier.

4.3.2 I-V Curve and Solar Cell Output Parameters

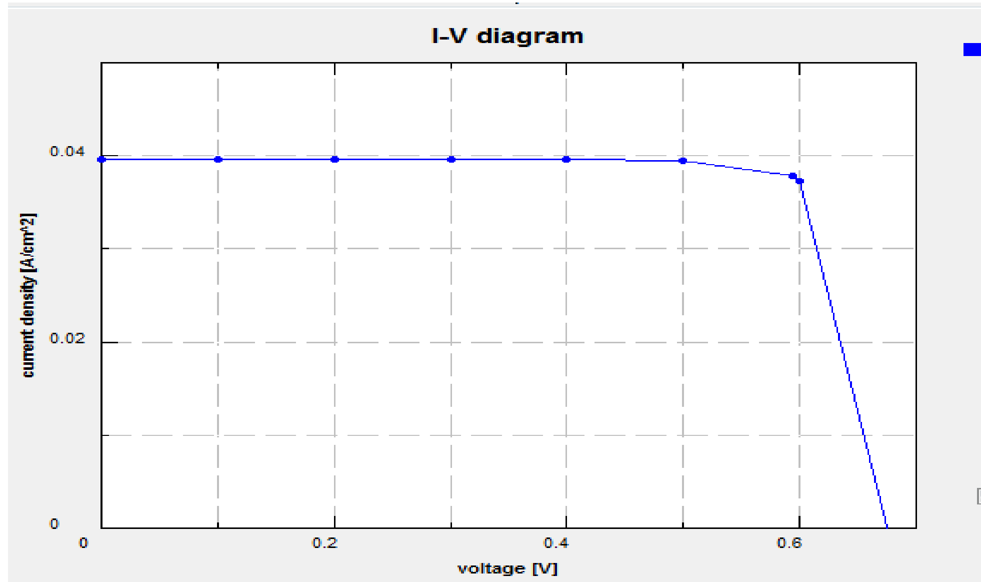

Figure 4.5 I-V curve for the graded structure

The solar cell output parameters are: V_{OC}=674.2 mV, J_{SC}= 37.95 mA/cm^2, FF= 83.94%, η= 21.47%.As we can see after inserting the graded band gap a-SiGe:H alloy as the intrinsic layer, the simulation results shows an increase in short circuit current and the overall efficiency also increase by about 3% (from 18.5% to 21.47%).

4.4 Comparison between Simple HIT and Proposed Structure:

The solar cell simulation results for the two structures are summarized in Table 3. When the results for the simple sturucture (Fig 3.2) and proposed structure (Fig 4.2) are compared, the open circuit voltage is much higher in the proposed sructure. The short-circuit current is slightly improved and the fill factor is also increased. As a results, the efficiency is increased by almost 3% when the a-Si:H is replaced by the graded a:SiGe:H layers in the structure.

Table 4.4 Comparison between the Simple HIT structure and the designed structure.

structure	**a-Si:H(n) thickness (nm)**	**a-Si:H(n) doping (cm^{-3})**	**c-Si(p) doping (cm^{-3})**	**i–layer thickness (nm)**	**V_{oc} (mV)**	**Jsc** (mA/cm^2)	**FF (%)**	**η (%)**
Simple HIT	10	1E20	1E16	5	639.8	37.61	76.87	18.5
Proposed structure	10	1E20	1E16	5	674.2	37.95	83.94	21.47

We also use AFORS-HET simulation software to optimize the different parameters of the structure to get a better and improved efficiency.

CHAPTER FIVE

OPTIMISATION OF THE STRUCTURE AND DISCUSSIONS

The doping concentration and the thickness of different layers in the Heterojunction with intrinsic thin layer solar cells influence their performances. So doping concentrations and thicknesses of n-layer, p-layer and i-layer are varied to see their influence in the performance of the solar cell and the best values has been selected to form an optimized structure with highest efficiency.

5.1 EFFECTS OF N-LAYER

The doping concentration and thickness of the n- layer has been varied to see the effect and find the optimized value

5.1.1 Optimization of n-layer thickness

The thickness of n-layer was varied from 0.5nm to 5nm and sees how it affects the output parameters of the solar cell. The simulation results are in Table 5.1

Table 5.1 Variation of n-layer thickness.

n-thickness (nm)	Voc (mV)	Jsc (mA/cm2)	FF (%)	ɳ (%)
0.5	641	39.5	76.7	19.41
1	641	39.4	76.7	19.37
1.5	641	39.3	76.7	19.33
2	641	39.2	76.7	19.29
2.5	641	39.1	76.7	19.25
3	641	39	76.7	19.21
3.5	641	38.9	76.7	19.16
4	641	38.8	76.7	19.12
4.5	641	38.7	76.7	19.08
5	641	38.6	76.7	19.04

The graph of the various output parameters are plotted against the thickness to see the variation of each with the increase in n-layer thickness

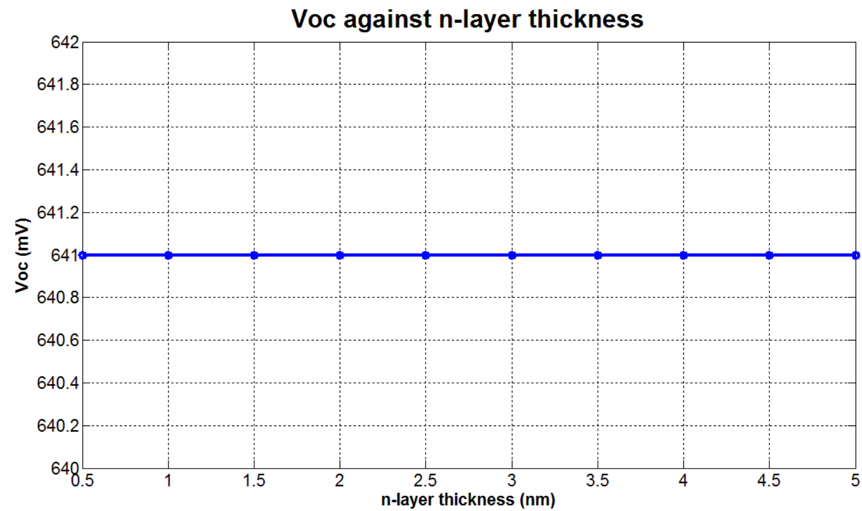

Figure 5.1 Variation of V_{OC} with n-layer thickness

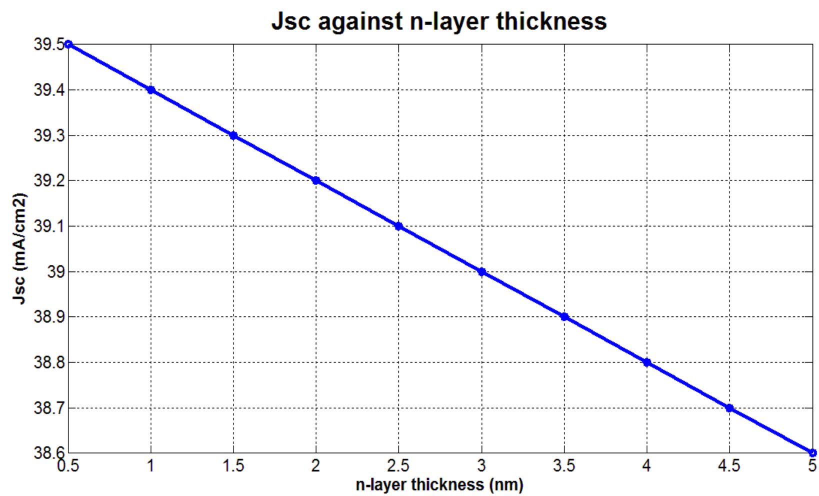

Figure 5.2 Variation of J_{SC} with n-layer thickness

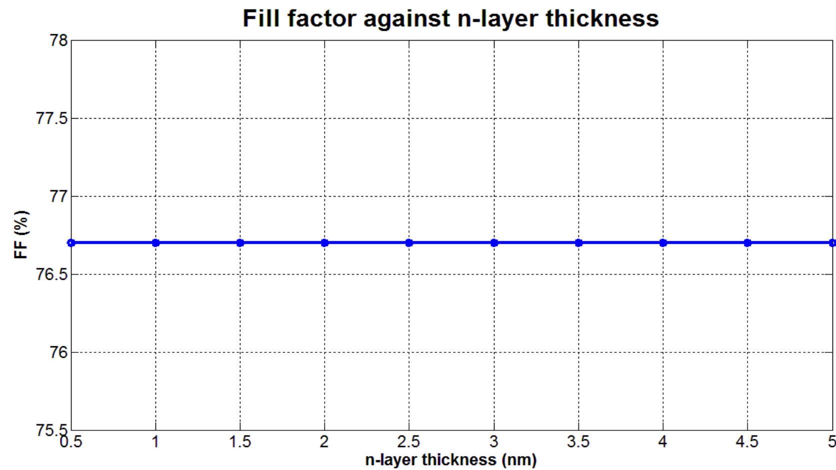

Figure 5.3 Variation of FF with n-layer thickness

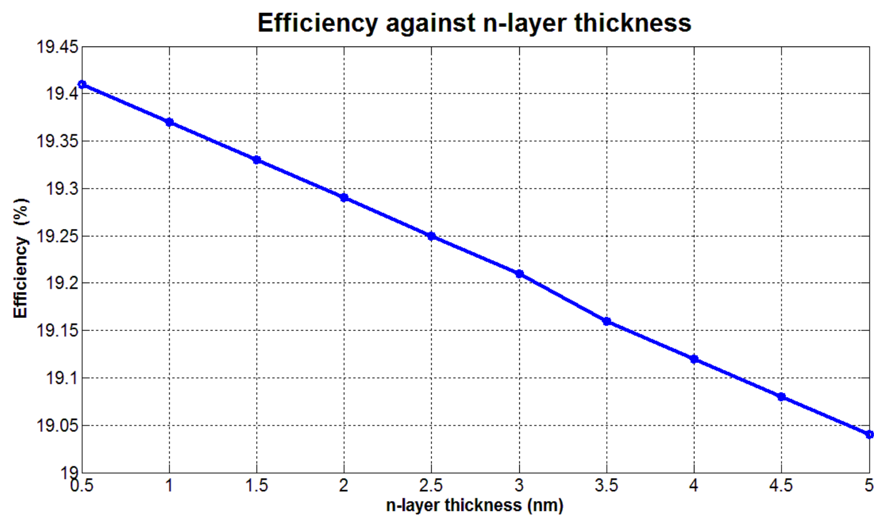

Figure 5.4 Variation of Efficiency with n-layer thickness

As can be seen from Figs 5.1-5.4, n-layer thickness does not have influence on the Voc and FF. Voc will be constant since the doping level is the same. On the other hand the Jsc is decreasing by increasing the n-layer thickness, this is because the n- layer is of a-si:H and it has defects which cause the increase in recombination at the layer, so when the layer is thicker the possibility of the recombination will increase, therefore the current is decrease by increasing the recombination which in turn decrease the efficiency. Therefore we try to make n-layer as thin as possible, so we choose 1nm as the optimized n-layer thickness.

5.1.2 Optimization of n-layer doping concentration

The doping concentration of the n- layer was varied in the range of 1E18,5E18, 1E19, 5E19 and 1E20. The simulation results and the graphs are shown below.

Table 5.2 Variation of n-layer doping concentration.

n-doping (cm^{-3})	Voc (mV)	Jsc (mA/cm^{-2})	FF (%)	η (%)
1.00E+18	757	46.04	85.04	29.64
5.00E+18	757	46.05	85.06	29.65
1.00E+19	757	46.05	85.07	29.66
5.00E+19	757	46.06	85.07	29.66
1.00E+20	757	46.05	85.07	29.66

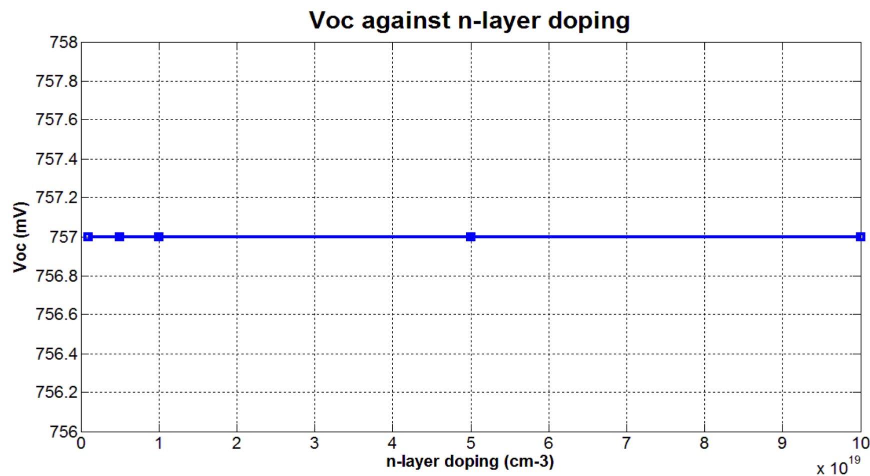

Figure 5.5 Variation of V_{OC} with n-layer doping

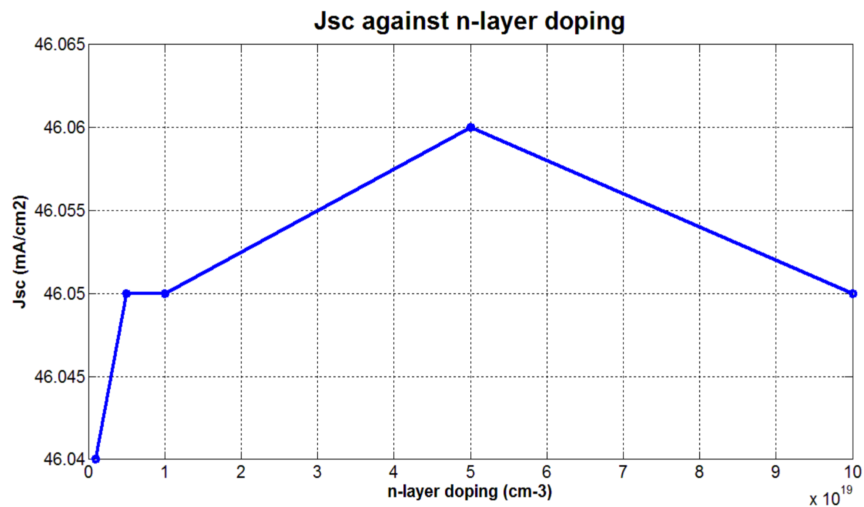

Figure 5.6 Variation of J_{SC} with n-layer doping

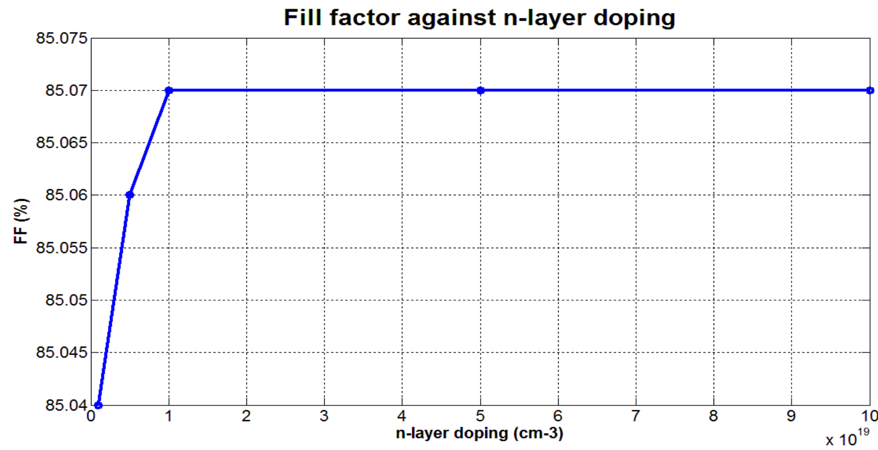

Figure 5.7 Variation of FF with n-layer doping

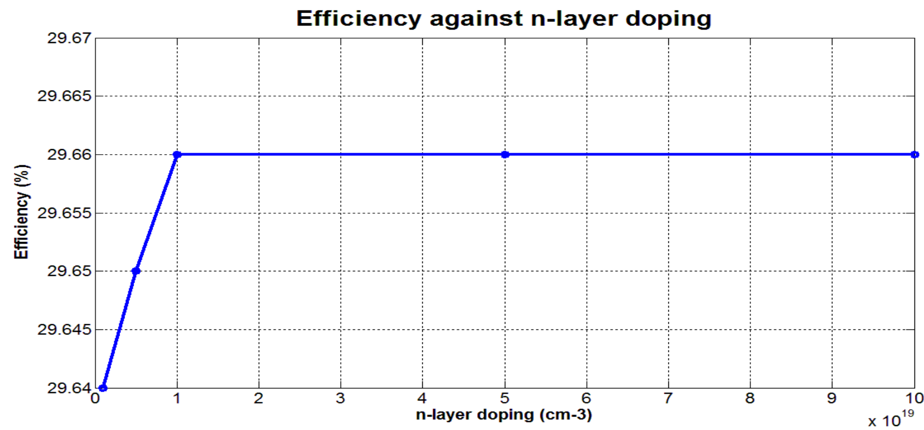

Figure 5.8 Variation of Efficiency with n-layer doping

As we can see from Figs 5.5-5.8 the V_{OC} is not affected with the n-layer doping but short circuit current increase to a certain value then saturate, we need a highly doped n-layer for wider depletion region. Therefore 1E20 was selected because the efficiency is high and the conductivity is highest. Increase in the conductivity will help reduce the series resistance on the n-side.

5.2 EFFECTS OF INTRINSIC LAYER

The intrinsic layer is an undoped thin buffer layer inserted in between a-Si:H and c-Si layers in heterojunction solar cell. The benefit of this layer is to reduce the interface defects when the heterointerface is formed. Normally the density of state in the undoped a-Si:H is

weaker than in doped a-Si:H, so by inserting the undoped layer the defect in between the undoped a-Si:H and c-Si the interface defects will be less.

5.2.1 Optimization of i-Layer Thickness

The thickness of the intrinsic layer was varied from 0.5nm to 3nm and the simulation results and the graphs for various output parameters are shown below

Table 5.3 variation of i-layer thickness

i-thickness (nm)	Voc (mV)	Jsc (mA/cm2)	FF (%)	η (%)
0.5	757	46.05	85.07	29.66
1	757	45.78	85.04	29.48
1.5	757	45.53	85.02	29.31
2	757	45.29	85.17	29.14
2.5	755.5	45.05	85.14	28.98
3	755.5	44.82	85.11	28.82

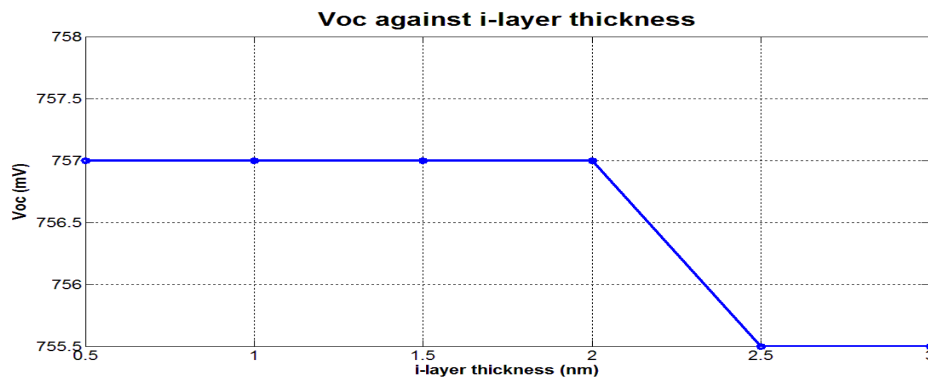

Figure 5.9 A graph showing Variation of V_{OC} with i-layer thickness

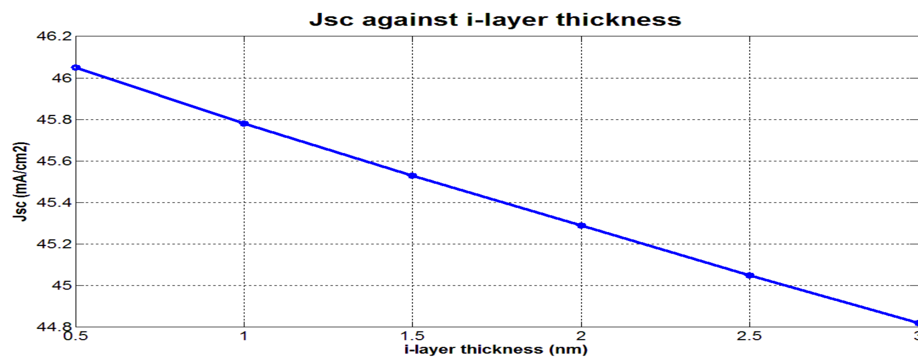

Figure 5.10 A graph showing variation of J_{SC} with i-layer thickness

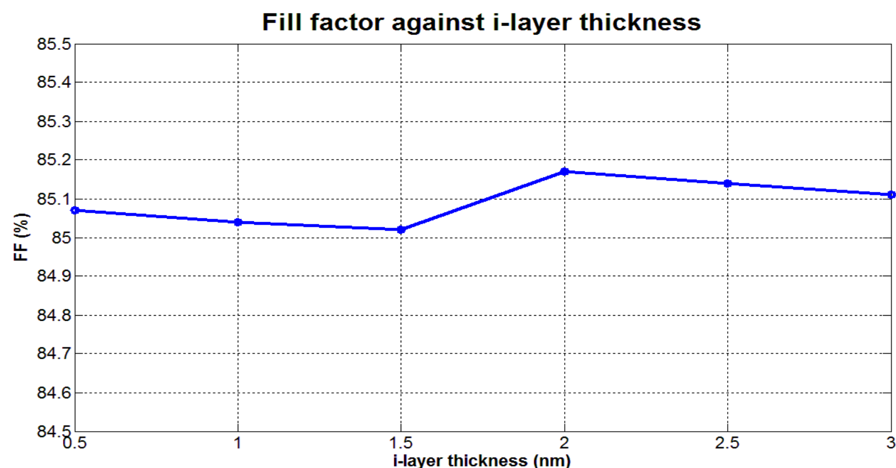

Figure 5.11 A graph showing variation of FF with i-layer thickness

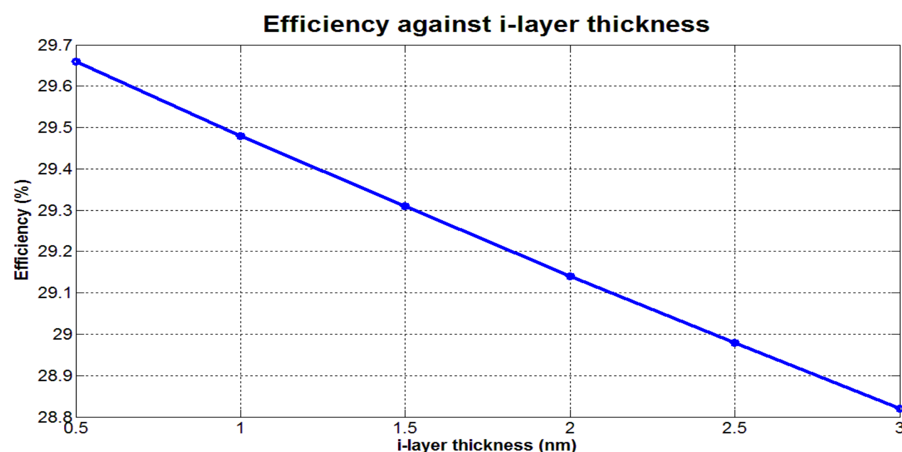

Figure 5.12 A graph showing variation of Efficiency with i-layer thickness

From Figs 5.9-5.12, we can see that the Jsc and Efficiency are decreasing with increasing the i-layer thickness while the Voc remains somehow constant. The reduction of efficiency is due to the low mobilities of electrons in the layer as well as high defects in the amorphous layer. That means the thinner the better, so the optimized thickness is 0.5 nm.

5.3 EFFECTS OF P-LAYER

The doping concentration and thickness of the p-layer has been varied to see the effect and find the optimized value.

5.3.1 Optimization of p-layer doping concentration

The p- doping was varied from 1E17 to1E18 and the simulation results were shown below. During our simulation we took the effect of mobilities in to consideration that is mobility is decreasing by increasing doping concentration in crystalline silicon.

Table 5.4 variation of p-doping taking mobilities effect in to consideration

p-doping (cm^{-3})	μ_e (cm^2/Vs)	μ_h (cm^2/Vs)	Voc (mV)	Jsc (mA/cm^2)	FF (%)	η (%)
1.00E+17	721	317	780.5	45.21	86.08	30.37
2.00E+17	560	266	768	46.94	85.23	30.73
3.00E+17	474	235	760.2	47.66	85.5	30.98
4.00E+17	419	214	757	47.91	85.26	30.93
5.00E+17	379	198	755.5	47.95	85.18	30.86
6.00E+17	349	185	755.5	47.92	85.12	30.81
7.00E+17	326	175	755.5	47.87	85.15	30.8
8.00E+17	306	166	757	47.82	85.07	30.79
9.00E+17	291	159	757	47.77	85.16	30.8
1.00E+18	277	153	757	47.72	85.25	30.8

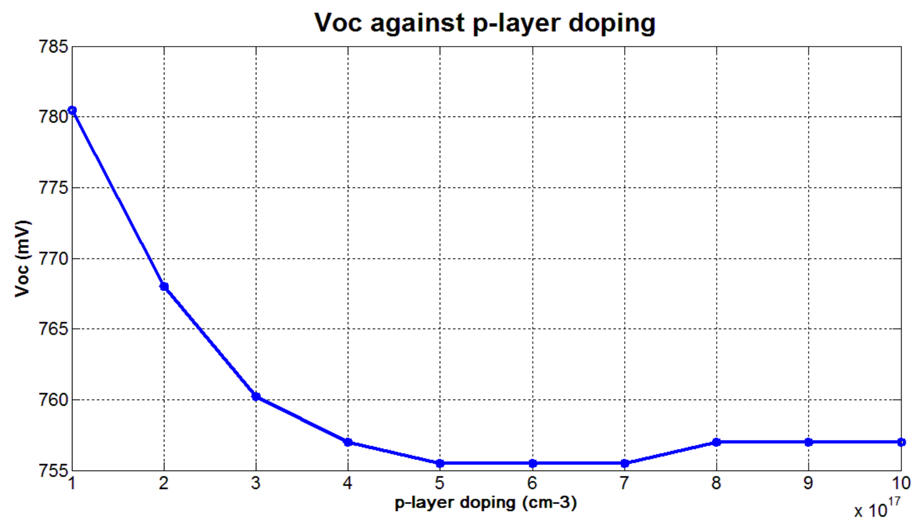

Figure 5.13A graph showing variation of V_{OC} with p-layer doping

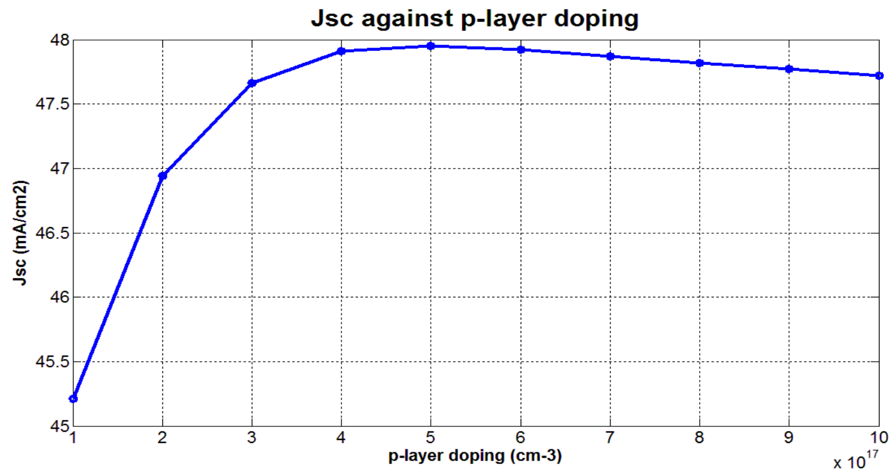

Figure 5.14Agraph showing variation of J_{SC} with p-layer doping

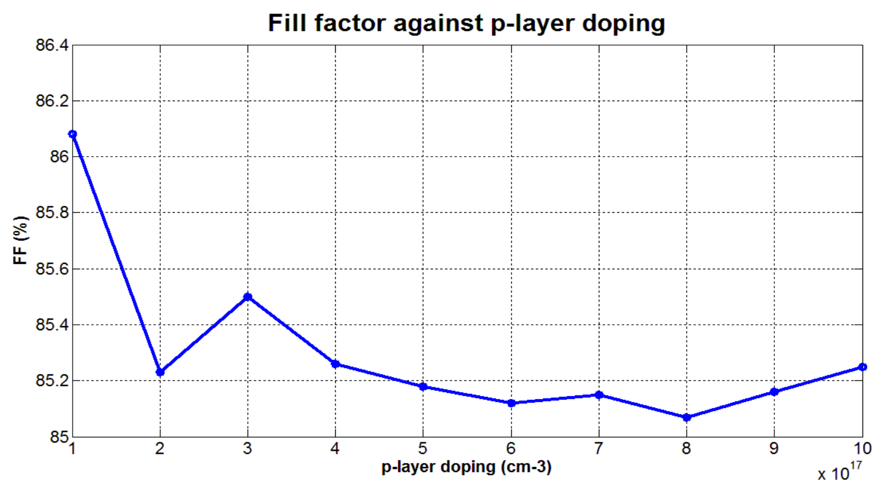

Figure 5.15A graph showing variation of FF with p-layer doping

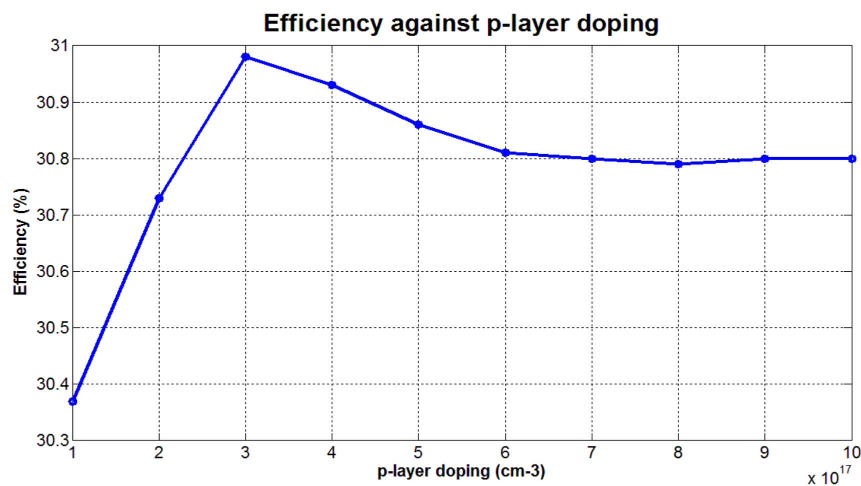

Figure 5.16 A graph showing variation of Efficiency with P-layer doping

We can see from Figs 5.13-5.16, how the parameters were varied with p-layer doping and the optimal value that gives the highest efficiency is 3E17.

5.3.2 Optimization of p-layer thickness

The thickness of p-layer was varied from 100μm to 500μm with 50μm increase and the simulation results with the graphs are shown below:

Table 5.5 variation of P-layer thickness

p-thickness (μm)	Voc (mV)	Jsc (mA/cm^2)	FF (%)	ɳ (%)
100	738.3	46.65	80.1	27.59
150	746.1	47.76	79.35	28.27
200	750.8	48.39	84.72	30.25
250	753.9	48.78	84.98	31.25
300	755.5	49.03	85.13	31.54
350	757	49.2	85.14	31.71
400	757	49.32	85.24	31.82
450	758	49.39	85.13	31.89
500	758.6	49.44	85.16	31.94

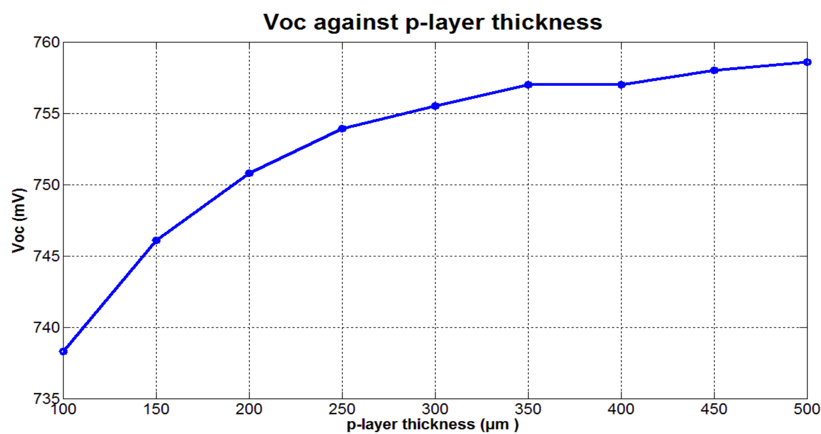

Figure 5.17A graph showing variation of V_{OC} with P-layer thickness

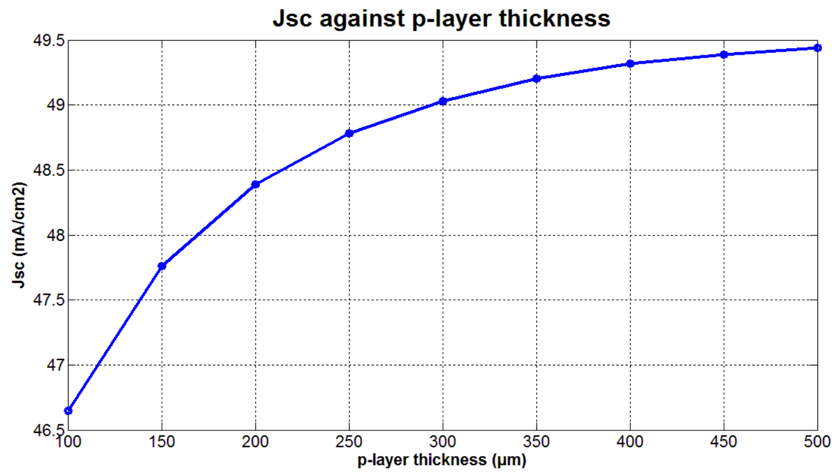

Figure 5.18A graph showing variation of JSC with P-layer thickness

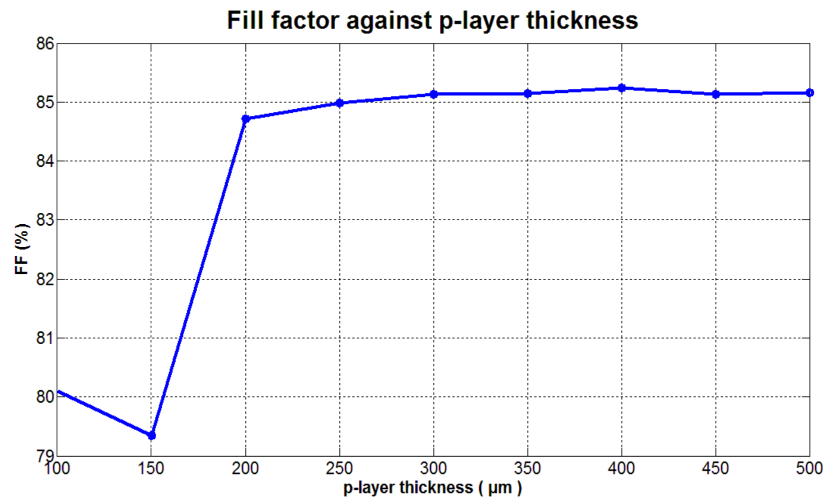

Figure 5.19A graph showing variation of FF with p-layer thickness

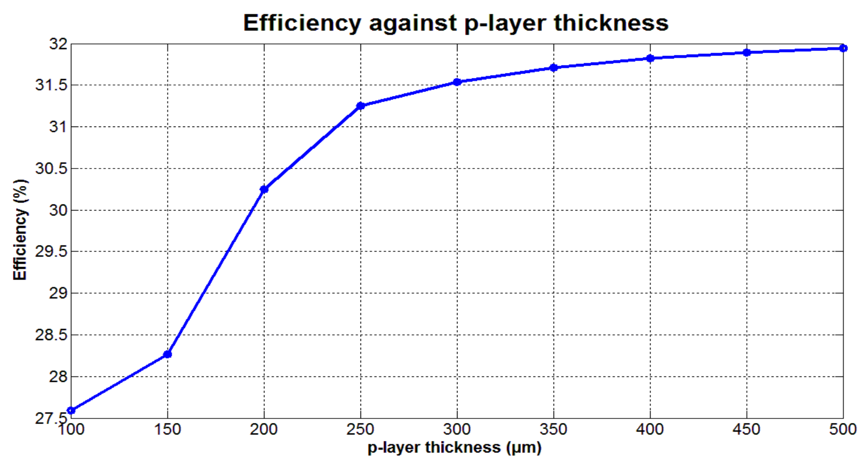

Figure 5.20 a graph showing variation of Efficiency with P-layer thickness

From Fig.5.20, Efficiency increases as the thickness of p-layer increases; this is due to increase in absorption. So, the thicker the p-layer the better the absorption, but we can note from the graph that after 300μm the increase is very small, so due to the cost of the wafer we need a p-layer to be as thin as possible. For the purpose of this work we choose the optimized p-thickness to be 300μm. the optimized parameters are shown in Table 5.6

Table 5.6 Optimized parameters for the structure

layer	doping	thickness
n	1E20 cm^{-3}	1 nm
i	-	0.5 nm
p	3E17 cm^{-3}	300 μm

5.4 EFFECTS OF TRANSPARENT CONDUCTING OXIDES (TCOs)

Different TCOs are used on the optimized structure to see the influence of each one in the performance of the solar cell. In this thesis, we use indium tin oxide (ITO) and zinc oxide (ZnO) but for each one we used textured and plane. The results of the simulations are shown in Table 5.7.

Table 5.7 Effects of TCOs

TCO	V_{OC} (mV)	J_{SC} (mA/cm^2)	FF (%)	η (%)
Plane ITO	752.3	40.15	84.88	25.64
Plane ZnO	755.5	44.54	85.09	28.63
Textured ITO	755.5	44.62	85.09	28.68
Textured ZnO	758.6	49.5	85.24	32.07

From the Table 5.7, ZnO textured gives a high efficiency of 32.07%, therefore the optimized structure will be: Textured ZnO/a-Si:H(n)/graded band gap a-SiGe:H(i)/c-Si(p)/Al with the above doping and thicknesses and our achieved efficiency is 32.07%

CHAPTER SIX

CONCLUSION AND FUTURE WORK

In this thesis, we worked on the problem of band offsets which occurs at the interface of a-Si:H and c-Si layers due to their electron affinity difference by designing a novel structure that contains an intrinsic graded band gap a-SiGe:H layer in between the two layers (a-Si:H and c-Si) which results in an increase in efficiency.

The proposed structure ZnO/a-Si:H(n)/graded-band-gap a-SiGe:H(i)/c-Si(p)/Al was simulated and the effect of doping concentration and thickness of the different layers on the performance of the solar cell was evaluated using AFORS-HET software.

For the optimized parameters, a record efficiency of 32.07% was obtained with the relevant parameters values of V_{OC}=758.6 mV, J_{SC}=49.5 mA/cm^2, FF=85.24%. These results were obtained from the following optimized values: Thickness of 1 nm, 0.5 nm and 300 µm for a-Si:H(n) (emitter-layer), graded band gap a-SiGe:H(i) (buffer layer) and c-Si(p) (absorber-layer), respectively. For doping concentrations, the optimized values are 1E20 and 1E18 for the emitter and absorber layers, respectively. Textured ZnO results in the highest efficiency for the TCO choice.

For the future work:

- The designed structure needs to be studied experimentally.
- Parameters of a-SiGe:H needs to be characterized.
- The solar cell devices have to be fabricated and tested.

REFERENCES

[1]International Energy Agency, *World Energy Outlook 2010* (2010).

[2] U.S. Energy Information Administration, *International Energy Outlook 2010* (2010).

[3] United Nations Population Information Network (POPIN),*World Population Prospects: The 2004 Revision Population Database* (2004).

[4] P. Crompton and Y. Wu, Energy Economics **27** (2005), 195.

[5] BP Statistical Review of World Energy 2010 (2010).

[6] K. Blok, *Introduction to Energy Analysis*, Techne Press, Amsterdam (2006).

[7] German Advisory Council on Global Change (WBGU), *World in Transition – Towards Sustainable Energy Systems* (2004).

[8] A.E. Becquerel, ComptesRendus de l'Academie des Sciences **9** (1839), 145.

[9] http://en.wikipedia.org/wiki/Solar_cell

[10] H.W. Schock, F. Pfister, Proceeding of the 16th European Photovoltaic Solar Energy Conference, pp.270-174, Glasgow, Germany, 2000.

[11] A.L Fahrenbruch, R.H.Bube, "Fundamentals of Solar Cells," Academic Press, 1983.

[12] M.L.Archer, R.Hill, "Clean Energy from Photovoltaics," Imperial College Press, 2001

[13] S. Metha, PV News **29-10** (2010), 3.

[14] S. Metha, PV News **30-5** (2011), 3.

[15] O. Schaefer, L. Torres and J. Blunden, Proc. of 25th EU PVSEC, Valencia, Spain (2010), 5235.

[16] http://www.setfor2020.eu

[17] W. Hoffmann and T. Pellkofer, Proc. of 25th EU PVSEC, Valencia, Spain (2010), 5217.

[18] S. Darula. L. Kittler and C.A. Gueymard, Solar Energy **79** (2005), 559.

[19] W.G.J.H.M. van Sark, G.W. Brandsen, M. Fleuster and M.P. Hekkert, Energy Policy **35** (2007), 3121.

[20] D.M. Chapin, C.S. Fuller and G.L. Pearson, J. Appl. Phys. **25** (1954), 676.

[21] J. Zhao, A. Wang and M.A. Green, Prog. Photovolt: Res. Appl. **7** (1999), 471.

[22] O. Schultz, S.W. Glunz and G.P. Willeke, Prog. Photovolt: Res. Appl. **12** (2004), 553.

[23] D.E. Carlson and C.R. Wronski, Appl. Phys. Lett. **28** (1976), 671.

[24] S. Benagli, D. Borrello, E. Vallat-Sauvain, J. Meier, U. Kroll, J. Hoetzel, J. Bailat, J. Steinhauser, M. Marmelo, G. Monteduro and L. Castens, Proc. of 24th EU PVSEC, Hamburg, Germany (2009), 2293.

[25] W.G.J.H.M. van Sark, Thin Films and Nanostructures **30** (2002), 1.98

[24] R.A. Street,*Hydrogenated Amorphous Silicon*, Cambridge University Press (1991).

[26] J.K. Rath, M. Brinza and R.E.I. Schropp, Proc. of 34th IEEE PVSC, Philadelphia, PA, USA (2009), 1196.

[27] Y. Liu, J.K. Rath and R.E.I. Schropp, Surf. Coat.Tech. **201** (2007), 9330.

[28] D.L. Staebler and C.R. Wronski, Appl. Phys. Lett. **31** (1977), 292.

[29] C.R. Wronski, B. von Roedern and A. Kolodziej, Vacuum **82** (2008), 1145.

[30] A. Gordijn, *Microcrystalline Silicon for Thin-Film Solar Cells*, Ph.D. Thesis, Utrecht University (2005).

[31] J. Meier, S. Dubail, R. Flückinger, D. Fischer, H. Keppner and A. Shah, Proc. of 1st WCPEC, Waikoloa, HI, USA (1994), 409.

[32] H. Li, R.H. Franken, R.L. Stolk, J.A. Schüttauf, C.H.M. van der Werf, J.K. Rath and R.E.I. Schropp, J. Non-Cryst. Sol. **354** (2008), 2445.

[33] R.E.I. Schropp, H. Li, R.H.J. Franken, J.K. Rath, C.H.M. van der Werf, J.A. Schüttauf and R.L. Stolk, Sol. Energy Mat. And Sol. Cells **93** (2009), 1129.

[34] B. Yan, G. Yue and S. Guha, Mater. Res. Soc. Symp. Proc. **989**, (2007), A15.01.

[35] B. Yan. G. Yue, X. Xu, J. Yang and S. Guha, Phys. Stat. Sol. A **207** (2010), 671.

[36] R.E.I. Schropp and M. Zeman, *Amorphous and Microcrystalline Silicon Solar Cells – Modeling, Materials and Device Technology*,Kluwer, Boston/Dordrecht/London (1998).

[37] S. Veprek and V. Marecek, Solid State Electron. **11** (1968), 683.99

[38] J. Meier, R. Flückiger, H. Keppner and A. Shah, Appl. Phys. Lett. **65** (1994), 860.

[39] K. Yamamoto, M. Toshimi, T. Suzuki, Y. Tawada, T. Okamoto and A. Nakajima, Mater. Res. Soc. Symp. Proc. **507** (1998), 131.

[40] J. Bailat, L. Fesquet, J-B.Orhan, Y. Djeridane, B. Wolf, P. Madliger, J. Steinhauser, S. Benagli, D. Borrello, L. Castens, G. Monteduro, M. Marmelo, B. Dehbozorghi, E. VallatSauvain, X. Multone, D. Romang, J-F. Boucher, J. Meier, U. Kroll, M. Despeisse, G. Bugnon, C. Ballif, S. Marjanovic, G. Kohnke, N. Borrelli, K. Koch, J. Liu, R. Modavis, D. Thelen, S. Vallon, A. Zakharian, and D. Weidman, Proc. of 25th EU PVSEC, Valencia, Spain (2010), 2720.

[41] M.A. Green, K. Emery, Y. Hishikawa and W. Warta, Prog. Photovolt: Res. Appl**19** (2011), 84.

[42] M.A. Green, *Solar Cells – Operating Principles, Technology and System Applications,* Prentice-Hall Inc., Englewood Cliffs, NJ, USA(1982).

[43] W. Fuhs, K. Niemann and J. Stuke, Bull. Am. Phys. Soc. **19** (1974),393.

[44] K. Okuda, H. Okamoto and Y. Hamakawa, Jpn. J. Appl. Phys. **22** (1983), L605.

[45] M. Tanaka, M. Taguchi, T. Matsuyama, T. Sawada, S. Tsuda, S. Nakano, H. Hanafusa and Y. Kuwano, Jpn. J. Appl. Phys. **31** (1992),3518.

[46] Y. Tsunomura, Y. Yoshimine, M. Taguchi, T. Baba, T. Kinoshita, H. Kanno, H. Sakata, E. Maruyama and M. Tanaka, Sol. Energy Mater. Sol. Cells **93** (2009), 670.

[47] R. Hulstrom, R. Bird and C. Riordan, Solar Cells **15** (1985), 365.

[48] M. Taguchi, K. Kawamoto, S. Tsuge, T. Baba, H. Sakata, M. Morizane, K. Uchihashi, N. Nakamura, S. Kiyama and O. Oota, Prog. Photovolt: Res. Appl. **8** (2000), 503.

[49] D. Lachenal, Y.Andrault, D. Bätzner, C. Guerin, M. Kobas, B. Mendes, B. Strahm, M. Tesfai, G. Wahli, A. Buechel, A. Descoeudres, G. Choong, R. Bartlome, L. Barraud, F. Zicarelli, P. Bôle, L. Fesquet, J. Damon-Lacoste, S. De Wolf and C. Ballif, Proc. of 25th EU PVSEC, Valencia, Spain (2010), 1272.

[50] National Renewable Energy Laboratory Website -http://rredc.nrel.gov/solar/spectra/am1.5/

[51] Website: http://www.greenrhinoenergy.com/solar/radiation/spectra.php

[52] M.A. Green, "*Solar Cells: Operating principles, technology, and system applications*", New Jersey: Prentice Hall 1982.

[53] S.R. Herd, P. Chaudhari, M.H. Brodsky, J. Non-Cryst. Solids 7 (1972) 309

[54] R. Stangl, C. Leendertz, J. Haschke (2010), *Numerical Simulation of Solar Cells and Solar Cell Characterization Methods: the Open-Source on Demand Program Afors-Het,* in*SolarEnergy*, [online], available at: http://www.intechopen.com/books/solarenergy/numerical-simulation-of-solar-cells-and-solar-cell-characterization-methods-theopen-source-on-demand

[55] W.G.J.H.M. van Sark, L. Korte and F. Roca, *Physics and Technology of Amorphous-Crystalline Heterostructure Silicon Solar Cells,* Berlin, Germany, Woodhead,2012.

[56] K.v. Maydell, E. Conrad, M. Schmidt, Efficient silicon heterojunction solar cells based on p- and n-type substrates processed attemperatures of 220 1C, Prog. Photovolt.Res. Appl. 14 (2006) 289.

[57] Stefaan Wolf De, Beaucarne Guy, Surface passivation properties of boron-doped plasma-enhanced chemical vapor deposited hydrogenated amorphous silicon films on p-type crystalline Si substrates, Appl. Phys. Lett. 88 (2006) 022104.

[58] Q. Wang, M.R. Page, E. Iwaniczko, Y.Q. Xu, L. Roybal, R. Bauer, D. Levi, Y.F. Yan, D. Meier, T.H. Wang, H.M. Branz, Silicon heterojunction solar cells by hot-wire CVD, in: ISES Solar World Congress, Beijing, China, 2007, pp. 1144–1147.

[59] B.M.Moustafa, B.Boumediene (2013), simulation and optimization of performance in Hit solar cell: international journal of computer applications (0975-8887) vol. 80-no 13.

[60] Luft W and Simon Tsuo Y 1993 *Hydrogenated Amorphous Silicon Alloy Deposition Process* (New York: MarcelDekker) p 27